Numerische Mathematik (2020) 146:281–334
https://doi.org/10.1007/s00211-020-01145-9

Numerische Mathematik

Transparent boundary conditions for wave propagation in fractal trees: convolution quadrature approach

Patrick Joly[1] · **Maryna Kachanovska**[1]

Received: 10 August 2019 / Revised: 3 August 2020 / Published online: 7 September 2020

Abstract
In this work we propose high-order transparent boundary conditions for the weighted wave equation on a fractal tree, with an application to the modeling of sound propagation in a human lung. This article follows the recent work (Joly et al. in Netw Heterog Media 14(2):205–264, 2019), dedicated to the mathematical analysis of the corresponding problem and the construction of low-order absorbing boundary conditions. The method proposed in this article consists in constructing the exact (transparent) boundary conditions for the semi-discretized problem, in the spirit of the convolution quadrature method developed by Ch. Lubich. We analyze the stability and convergence of the method, and propose an efficient algorithm for its implementation. The exposition is concluded with numerical experiments.

Mathematics Subject Classification 65M12 · 65M60 · 65M06 · 35R02

1 Introduction

Sound propagation in a human lung can be used for non-invasive diagnosis of the respiratory diseases, see e.g. [44] for some experimental studies, a PhD thesis [25], and, in particular, the Audible Human Project [47] and references therein. A human lung can be viewed as a network of small tubes (bronchioles), immersed into the lung tissue (parenchyma) and coupled with their ends to microscopic cavities in the parenchyma (alveoli). The physical phenomenon of sound propagation in a lung is highly complex, due to the fractal geometry of lung airways, heterogeneity of parenchyma, interactions/couplings between various types of tissues, and, eventually, multiscale nature of

✉ Maryna Kachanovska
maryna.kachanovska@inria.fr

Patrick Joly
patrick.joly@inria.fr

[1] POEMS (INRIA-CNRS-ENSTA), Institut Polytechnique de Paris, 828 Boulevard des Maréchaux, 91120 Palaiseau, France

the problem. Thus, in practice, one uses simplified models. For instance, in the mathematical literature, in [12,13], sound propagation in a highly heterogeneous parenchyma is modelled using the homogenization techniques. In [40] Sobolev spaces associated to the Laplace equation on a fractal tree that models the network of bronchioli are studied, and in [21] the wave equation with a viscous non-local term on a dyadic infinite tree is analyzed, see as well the monograph [39]. This point of view at the bronchioli as a self-similar network (with possibly multiple levels of self-similar structure) seems to be rather classical (though indeed simplified) in the medical and medical engineering literature, see in particular [16,26,42,48] for the related discussion. In this article we adapt this, simplified, approach of studying wave propagation in lungs.

In the limit when the thickness of the bronchiolar tubes tends to zero, the problem becomes essentially one-dimensional inside each of the tubes. A rigorous asymptotic analysis [34,46] allows to take into account the differences between the thicknesses of the tubes at different levels of the bronchiolar tree via incorporating weights into the originally homogeneous wave equation. Constructing an efficient numerical method for the resolution of such a 1D weighted wave equation defined on a fractal tree is the subject of the present work. In the literature [8] the type of problems we consider is sometimes referred to as problems posed on a metric graph, to underline the distinction between this kind of models and discrete, finite-difference-like models on graphs.

This problem gives rise to numerous interesting questions from the analytical (relations between associated weighted Sobolev spaces on fractal trees, in particular, embeddings and existence of a trace), and from the numerical point of views (since the fractal tree has an infinite number of edges). The analysis related questions have been answered in [33], while the construction of efficient numerical methods for such problems is mainly the subject of the present work. Our principal idea is to construct transparent boundary conditions for the wave propagation in a fractal tree, which would allow to perform all the computations on a truncated tree. Note that the transparent boundary conditions in the present article can be extended to the case when the whole tree $\mathcal{T}$ is not fractal, provided that after a certain generation, all of its subtrees are (as defined [33]). Most of such boundary conditions are based on an approximation of the Dirichlet-to-Neumann (DtN) operator.

In this work we construct an exact DtN operator for a semi-discretized in time system, in the spirit of the convolution quadrature (CQ) methods [37,38], see in particular numerous recent works dedicated to the coupling of boundary integral equations and volumic wave equations (FEM–BEM coupling) [6,24,36,41]. Let us mention a related approach, based on constructing transparent boundary conditions for problems discretized in space and time, see e.g. [2,9–11,35] and references therein. Our transparent boundary conditions can be viewed as Johnson–Nédélec style coupling [28], which was, in the context of the acoustic wave equation, studied in the PhD thesis [22], or, for the Schrödinger equation, in [45]. In this work we perform the convergence and stability analysis for such a coupling.

In view of the abundance of the literature on the numerical methods for similar wave problems, let us discuss the novel aspects of the work.

First of all, up to our knowledge, no work in the literature was devoted to the design of numerical method for time domain wave propagation in fractal trees, together with the development of the corresponding rigorous analysis. We have been developing

simultaneously two competing approaches for dealing with this kind of problems: high order local approximations of the DtN map [31,32] and adaptation of the convolution quadrature method, which is the subject of the present article. Let us remark that from the point of view of physics, the problem that we consider is different from the classical setting of the wave equation in the free space. The 'infinite' boundary of the fractal tree reflects waves, rather than absorbs them (i.e. loosely speaking the problem is more similar to the wave equation on the interval than the wave equation in the free space). It is therefore more advantageous to use non-dissipative discretization methods (e.g. trapezoid rule convolution quadrature).

Second, concerning the contribution to the convolution quadrature itself, we would like to cite a few novel aspects of this work:

- in the problem that we consider, neither the convolution kernel, nor its Fourier–Laplace transform are known in a closed form (unlike many other applications of the CQ). We thus propose an efficient procedure for its approximation, suitable for the use in the convolution quadrature.
- for the sake of efficiency, we use an explicit leapfrog time discretization for the volumic terms and an implicit trapezoid rule discretization for the boundary terms. This is different from the existing works [24,41] where for the discretization purely implicit schemes were used. From this point of view, the closest existing paper is the one by Banjai et al. [6]. However, we work with a different type of volumic-interface coupling. Moreover, because of the combination of the discretization schemes used in our work, there is no need for a stabilization term (unlike in [6]).
- finally, the full convergence analysis of the trapezoid rule (which we use here) for boundary operators occurring in wave problems is much less developed compared to the analysis of the L-stable Runge–Kutta methods. The complete convergence estimates (explicit in time) have been established only very recently, cf. [20], based on the Laplace domain estimates; the same is true for the coercivity preserving properties, cf. [5]. It is nonetheless not clear whether the error bounds of [20] are optimal. In the present work we perform the analysis purely in the time domain (unlike e.g. [6,36]); numerical experiments indicate that our error bounds are close to optimal (we lose only one power of the final simulation time T in the estimates).

This article is organized as follows. In Sect. 2 we recall the notation and formulate the problem. Section 3 is dedicated to the construction of transparent boundary conditions, as well as their analysis (stability and convergence). In Sect. 4 we provide algorithmic aspects of the method and perform its complexity analysis. Finally, Sect. 5 is dedicated to the numerical experiments. We conclude with a discussion of the obtained results in Sect. 6.

2 Problem setting

2.1 Notation

We will adhere to the notation and terminology used in [33]. Let us recall some of the geometric assumptions:

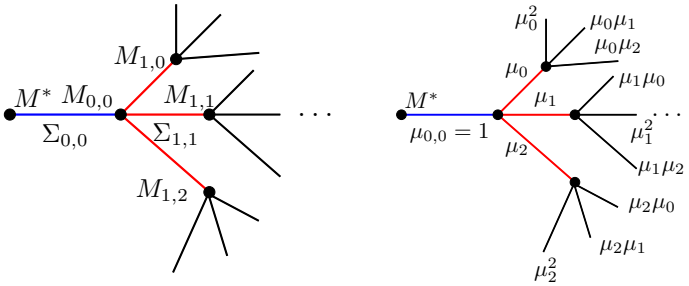

Fig. 1 A self-similar 3-adic infinite tree. Left: in blue we mark the edges that belong to $\mathcal{G}^0$, in red the edges of $\mathcal{G}^1$, in black the edges of $\mathcal{G}^2$. Right: distribution of weights on the edges of a 3-adic infinite self-similar tree (color figure online)

1. By $\mathcal{T}$ we will denote a p-adic rooted tree with infinitely many edges and no leaves. These edges are ordered in generations (collections of edges) $\mathcal{G}^i$ in the following manner: $\mathcal{G}^0$ consists of a root edge (where by the root edge we mean an edge whose one of the vertices is the root vertex); $\mathcal{G}^{n+1}$ is a union of children edges of all the edges from the generation $\mathcal{G}^n$. Each generation $\mathcal{G}^n$, $n \in \mathbb{N}$, contains p^n edges $\Sigma_{n,k}$, $k = 0, \dots, p^n - 1$.
   The children of the edge $\Sigma_{n,k}$ (of the generation $n+1$) are indexed as
   $$\Sigma_{n+1,pk+j}, \quad j = 0, \dots, p-1. \tag{1}$$
   The root vertex of the tree is denoted by M^*. We will study metric trees. This means that each edge of the tree $\Sigma_{n,k}$ can be viewed as a line segment of non-zero length. This allows to introduce a distance $d(M, M^*)$ between a vertex M and the root vertex M^* as the length of the path between M and M^*, i.e. the sum of the lengths of the edges that connect M and M^*. Then, provided that the edge $\Sigma_{n,k}$ is incident to two vertices M_0, M_1, we denote by $M_{n,k} = \operatorname{argmax}_{V \in \{M_0, M_1\}} d(V, M^*)$. See Fig. 1, left, for an illustration.
2. Each edge $\Sigma_{n,k}$ is assigned its length $\ell_{n,k} > 0$ and a weight $\mu_{n,k} > 0$.
3. We will assume that the tree is self-similar (fractal), in the sense of [33, Definition 2.3]. Let us explain this in more details. Let
   $$\boldsymbol{\alpha} = \big(\alpha_0, \dots, \alpha_{p-1}\big) \text{ and } \boldsymbol{\mu} = \big(\mu_0, \dots, \mu_{p-1}\big)$$
   be two vectors with positive elements. Then the length $\ell_{n+1,pk+j}$ and the weight $\mu_{n+1,pk+j}$ of the edge $\Sigma_{n+1,pk+j}$ are related to the length and the weight of the parent edge $\Sigma_{n,k}$, cf. (1), as follows:
   $$\ell_{n+1,pk+j} = \alpha_j \, \ell_{n,k}, \quad \mu_{n+1,pk+j} = \mu_j \mu_{n,k} \quad j = 0, \dots, p-1.$$
   Without loss of generality, we will assume that $\mu_{0,0} = 1$. An illustration to the above is given in Fig. 1, right.

Finally, we will denote by $\mathcal{T}^m$ the subtree of $\mathcal{T}$ truncated to $m+1$ generations, whose edges are given by a collection

$$\mathcal{T}^m := \{\Sigma_{n,k},\ 0 \le k \le p^n - 1,\ 0 \le n \le m\} \equiv \bigcup_{\ell=0}^{m} \mathcal{G}^\ell. \tag{2}$$

By $\mathcal{T}_{m,j}$ we will denote a p-adic infinite subtree of the tree $\mathcal{T}$, whose root edge is $\Sigma_{m,j}$. All over the article we will assume that $|\boldsymbol{\alpha}|_\infty := \sup |\alpha_j| < 1$ (i.e. the tree can be compactly embedded into $\mathbb{R}^d$, $d \ge 1$). We will refer to a weighted tree $\mathcal{T}$ as to a reference tree if the length of its root edge satisfies $\ell_{0,0} = 1$.

2.2 Wave propagation in self-similar weighted trees

We consider the problem of wave propagation on a self-similar weighted reference tree $\mathcal{T}$. For this we introduce a parametrization of each edge $\Sigma_{n,j}$ of the tree, incident to the vertices $M^*_{n,j}$, $M_{n,j}$, by an abscissa $s_{n,j} \in [0, \ell_{n,j}]$, with $\ell_{n,j}$ being the length of the edge. This parametrization is chosen so that 0 is associated to the vertex $M^*_{n,j}$ and $\ell_{n,j}$ to the vertex $M_{n,j}$. With s being an abscissa on the tree $\mathcal{T}$, defined on each edge $\Sigma_{n,j}$ as above, we define the weight function $\mu(s)$ on $\mathcal{T}$, with an abuse of notation:

$$\mu(s) = \mu_{n,j}, \quad s \in \Sigma_{n,j}.$$

An acoustic pressure $u : \mathcal{T} \times \mathbb{R}^+ \to \mathbb{R}$ (here $\mathbb{R}^+ = [0, \infty)$) satisfies the weighted wave equation, which can be written in a compact manner as

$$\mu\, \partial_t^2 u - \partial_s(\mu\, \partial_s u) = \widetilde{f}, \quad u(.,0) = \partial_t u(.,0) = 0, \tag{3}$$

with $\widetilde{f} : \mathcal{T} \times \mathbb{R}^+ \to \mathbb{R}$ being a source term. We equip this problem with a boundary condition at the root vertex $u(M^*, t) = 0$. It remains to pose the boundary conditions at the 'infinite' boundary of $\mathcal{T}$, the meaning of which will become clear in Sect. 2.3. For the moment, let us explain in detail the meaning behind (3). With the notation $u_{n,j} = u|_{\Sigma_{n,j}}$, from (3) it follows that:

$$\partial_t^2 u_{n,j} - \partial_s^2 u_{n,j} = f_{n,j} \quad \text{on } \Sigma_{n,j}, \quad j = 0, \dots p^n - 1, \quad n \ge 0, \tag{4}$$

$$u(.,0) = \partial_t u(.,0) = 0, \quad u(M^*, t) = 0, \tag{5}$$

where $f_{n,j}$ is the restriction of $\mu^{-1}\widetilde{f}$ to $\Sigma_{n,j}$. It is equipped with the continuity ($\mathcal{C}$) and Kirchoff ($\mathcal{K}$) conditions in all the vertices, cf. (1),

$$u_{n,j}(M_{n,j}, t) = u_{n+1,pj+k}(M_{n,j}, t), \quad k = 0, \dots, p-1, \tag{$\mathcal{C}$}$$

$$\partial_s u_{n,j}(M_{n,j}, t) = \sum_{k=0}^{p-1} \mu_k\, \partial_s u_{n+1,pj+k}(M_{n,j}, t), \quad j = 0, \dots p^n - 1,\ n \ge 0. \tag{$\mathcal{K}$}$$

2.3 Dirichlet and Neumann problems at the fractal boundary of the tree

The problem (4, 5, $\mathcal{C}$, $\mathcal{K}$) needs to be equipped with boundary conditions at the fractal boundary of the tree. This becomes more clear when studying the family of problems (3) posed on subtrees $\mathcal{T}^m$, $m \to \infty$: for their well-posedness, it is necessary to define boundary conditions on the 'outer' boundary of the tree $\mathcal{T}^m$, i.e. vertices $\{M_{m,j},\ j = 0, \dots, p^m - 1\}$. This will be done variationally, by introducing the associated Sobolev spaces.

2.3.1 Sobolev Spaces on $\mathcal{T}$

Given a function $v = v(s)$, $v : \mathcal{T} \to \mathbb{R}$, let

$$\int_{\mathcal{T}} \mu\, v := \sum_{n=0}^{\infty} \sum_{k=0}^{p^n-1} \int_{\Sigma_{n,k}} \mu_{n,k}\, v(s) ds.$$

We will need the following three spaces:

– square-integrable functions

$$\mathrm{L}^2_\mu(\mathcal{T}) = \left\{ v :\ v|_{\Sigma_{n,j}} \in \mathrm{L}^2(\Sigma_{n,j}),\ \|v\|_{\mathrm{L}^2_\mu(\mathcal{T})} < \infty \right\},$$
$$\|v\|^2_{\mathrm{L}^2_\mu(\mathcal{T})} = \|v\|^2 = \int_{\mathcal{T}} \mu |v|^2, \quad (v, g) := \int_{\mathcal{T}} \mu\, v\, g.$$

– square-integrable continuous functions with square-integrable derivatives: denoting by $C(\mathcal{T})$ continuous functions on $\mathcal{T}$,

$$\mathrm{H}^1_\mu(\mathcal{T}) := \left\{ v \in C(\mathcal{T}) \cap \mathrm{L}^2_\mu(\mathcal{T}) : |v|_{\mathrm{H}^1_\mu(\mathcal{T})} < \infty \right\},$$
$$|v|_{\mathrm{H}^1_\mu(\mathcal{T})} \equiv \|\partial_s v\|_{\mathrm{L}^2_\mu(\mathcal{T})}, \quad \|v\|^2_{\mathrm{H}^1_\mu(\mathcal{T})} = \|v\|^2_{\mathrm{L}^2_\mu(\mathcal{T})} + |v|^2_{\mathrm{H}^1_\mu(\mathcal{T})}.$$

– the closure of compactly supported H^1_μ-functions. For this let us define

$$\mathrm{H}^1_{\mu,\mathrm{c}}(\mathcal{T}) := \left\{ v \in \mathrm{H}^1_\mu(\mathcal{T}) :\ v = 0 \text{ on } \mathcal{T} \backslash \mathcal{T}^m, \text{ for some } m \in \mathbb{N} \right\},$$

i.e. functions which are supported inside $\mathcal{T}^m$, for some $m \in \mathbb{N}$. Then

$$\mathrm{H}^1_{\mu,0}(\mathcal{T}) := \overline{\mathrm{H}^1_{\mu,\mathrm{c}}(\mathcal{T})}^{\|.\|_{\mathrm{H}^1_\mu(\mathcal{T})}}.$$

The above definitions can be naturally extended to the spaces defined on a truncated tree $\mathcal{T}^m$, with an associated L^2_μ-scalar product denoted by $(.,.)_{\mathcal{T}^m}$.

Remark 2.1 All over this article we work with real-valued function spaces in the time domain, and with complex-valued function spaces in the frequency domain (as this is clear from the context, we do not provide explicit indications).

2.3.2 The evolution problems in weak form

It is easily seen that any $\mathrm{H}^1_\mu(\mathcal{T})$-solution of (4, $\mathcal{C}$, $\mathcal{K}$) satisfies

$$\left(\partial_t^2 u, v\right) + (\partial_s u, \partial_s v) = (f, v), \quad \text{for all } v \in \mathrm{H}^1_{\mu,\mathrm{c}}(\mathcal{T}), \text{ s.t. } v(M^*) = 0.$$

Reciprocally, any $\mathrm{H}^1_\mu(\mathcal{T})$-solution to the above problem solves (4, $\mathcal{C}$, $\mathcal{K}$).

To distinguish the Dirichlet and Neumann problems for (3), let us introduce

$$V_{\mathfrak{n}}(\mathcal{T}) = \left\{ v \in \mathrm{H}^1_\mu(\mathcal{T}) : v(M^*) = 0 \right\}, \quad V_{\mathfrak{d}}(\mathcal{T}) = \left\{ v \in \mathrm{H}^1_{\mu,0}(\mathcal{T}) : v(M^*) = 0 \right\}.$$

Definition 2.1 (*Neumann problem*) Find

$$u_{\mathfrak{n}} \in C\left(\mathbb{R}^+; V_{\mathfrak{n}}(\mathcal{T})\right) \cap C^1\left(\mathbb{R}^+; \mathrm{L}^2_\mu(\mathcal{T})\right),$$

s.t. $u_{\mathfrak{n}}(.,0) = \partial_t u_{\mathfrak{n}}(.,0) = 0$, and, for all $t > 0$,

$$\left(\partial_t^2 u_{\mathfrak{n}}, v\right) + (\partial_s u_{\mathfrak{n}}, \partial_s v) = (f, v), \quad \text{for all } v \in V_{\mathfrak{n}}(\mathcal{T}). \tag{N}$$

Definition 2.2 (*Dirichlet problem*) Find

$$u_{\mathfrak{d}} \in C\left(\mathbb{R}^+; V_{\mathfrak{d}}(\mathcal{T})\right) \cap C^1\left(\mathbb{R}^+; \mathrm{L}^2_\mu(\mathcal{T})\right),$$

s.t. $u_{\mathfrak{d}}(.,0) = \partial_t u_{\mathfrak{d}}(.,0) = 0$, and, for all $t > 0$,

$$\left(\partial_t^2 u_{\mathfrak{d}}, v\right) + (\partial_s u_{\mathfrak{d}}, \partial_s v) = (f, v), \quad \text{for all } v \in V_{\mathfrak{d}}(\mathcal{T}). \tag{D}$$

Remark 2.2 Although, strictly speaking, the problem (N) is a mixed problem (because of the Dirichlet condition at the root of $\mathcal{T}$), we call it 'Neumann', since we are interested in the behaviour at the fractal boundary of $\mathcal{T}$.

These problems are well-posed, as summarized below.

Theorem 2.1 *Let $f \in L^1_{loc}(\mathbb{R}^+; \mathrm{L}^2_\mu(\mathcal{T}))$. Then the problem (N) (resp. (D)) has a unique solution*

$$u_{\mathfrak{a}} \in C\left(\mathbb{R}^+; V_{\mathfrak{a}}(\mathcal{T})\right) \cap C^1\left(\mathbb{R}^+; \mathrm{L}^2_\mu(\mathcal{T})\right), \quad \mathfrak{a} = \mathfrak{n} \text{ (resp. } \mathfrak{a} = \mathfrak{d}).$$

Moreover, there exists $C > 0$, s.t. for all $T > 0$ and $0 \le t \le T$,

$$\|\partial_t u_{\mathfrak{a}}(t)\|_{\mathrm{L}^2_\mu(\mathcal{T})} + \|\partial_s u_{\mathfrak{a}}(t)\|_{\mathrm{L}^2_\mu(\mathcal{T})} \le C \|f\|_{L^1\left(0,T;\mathrm{L}^2_\mu(\mathcal{T})\right)}. \tag{6}$$

Proof The proof is classical. The existence and uniqueness result follows from the semigroup theory (see in particular [43, Section 4.2] and [43, Section 7.4]). To show (6), one first tests e.g. (N) with $\partial_t u_{\mathfrak{n}}$, which gives

$$\frac{d}{dt}\mathcal{E}_{\mathfrak{n}}(t) = (f, \partial_t u_{\mathfrak{n}}), \quad \mathcal{E}_{\mathfrak{n}} = \frac{1}{2}\left(\|\partial_t u_{\mathfrak{n}}\|^2 + \|\partial_s u_{\mathfrak{n}}\|^2\right).$$

The application of a Gronwall inequality (cf. [30, Appendix E]) yields the desired result. □

To state the following result, let us recall that, provided a Banach space X, the spaces $W^{k,1}_{loc}(\mathbb{R}^+; X)$ of X-valued distributions are defined as follows:

$$W^{k,1}_{loc}(\mathbb{R}^+; X) = \left\{ v : \mathbb{R}^+ \to X \text{ s.t. } \int_0^T \sum_{j=0}^{k} \left\| \partial_t^j v(t) \right\|_X dt < \infty, \ \forall\, T > 0 \right\}.$$

Corollary 2.1 *Let $k \geq 1$, $f \in W^{k,1}_{loc}(\mathbb{R}^+; \mathrm{L}^2_\mu(\mathcal{T}))$ and $f(0) = \cdots = \partial_t^{k-1} f(0) = 0$. Then*

$$u_{\mathfrak{a}} \in C^k\left(\mathbb{R}^+; V_{\mathfrak{a}}(\mathcal{T})\right) \cap C^{k+1}\left(\mathbb{R}^+; \mathrm{L}^2_\mu(\mathcal{T})\right), \quad \mathfrak{a} \in \{\mathfrak{d}, \mathfrak{n}\}.$$

Moreover, there exists $C > 0$, s.t. for all $0 \leq \ell \leq k$, all $T > 0$ and $0 \leq t \leq T$, it holds:

$$\left\| \partial_t^{\ell+1} u_{\mathfrak{a}}(t) \right\|_{\mathrm{L}^2_\mu(\mathcal{T})} + \left\| \partial_s \partial_t^{\ell} u_{\mathfrak{a}}(t) \right\|_{\mathrm{L}^2_\mu(\mathcal{T})} \leq C \left\| \partial_t^{\ell} f \right\|_{L^1\left(0,T;\mathrm{L}^2_\mu(\mathcal{T})\right)}. \tag{7}$$

Proof The function $\varphi = \partial_t^\ell u_{\mathfrak{a}}$, $0 \leq \ell \leq k$, solves the problem (N) (resp. (D)) with f replaced by $f^{(\ell)} \in L^1(\mathbb{R}^+; \mathrm{L}^2_\mu(\mathcal{T}))$, hence Theorem 2.1 applies. □

It is natural to ask whether the solutions to (N) and (D) coincide (like in the case $p = 1$, $\mu = 1$ and $\alpha = 1$, when $\mathcal{T}$ can be identified with $\mathbb{R}^+$). The answer depends on the following two quantities:

$$\langle \boldsymbol{\mu}\boldsymbol{\alpha} \rangle := \sum_{i=0}^{p-1} \mu_i \alpha_i, \quad \left\langle \frac{\boldsymbol{\mu}}{\boldsymbol{\alpha}} \right\rangle \equiv \langle \boldsymbol{\mu}/\boldsymbol{\alpha} \rangle := \sum_{i=0}^{p-1} \frac{\mu_i}{\alpha_i}.$$

Theorem 2.2 ([33]) *If $\langle \boldsymbol{\mu}\boldsymbol{\alpha} \rangle \geq 1$ or $\langle \boldsymbol{\mu}/\boldsymbol{\alpha} \rangle \leq 1$, $\mathrm{H}^1_{\mu,0}(\mathcal{T})$ and $\mathrm{H}^1_\mu(\mathcal{T})$ coincide, and thus $u_{\mathfrak{n}} = u_{\mathfrak{d}}$. Otherwise, $\mathrm{H}^1_{\mu,0}(\mathcal{T}) \subsetneq \mathrm{H}^1_\mu(\mathcal{T})$, and $u_{\mathfrak{n}} \neq u_{\mathfrak{d}}$.*

2.4 Transparent boundary conditions

In [33] it was shown how to construct transparent boundary conditions for the problems (N), (D). To recall the main ideas, we fix $m \geq 1$, and assume that

Assumption 2.1 The source $f(s,t)$ is s.t. for all $t \geq 0$, supp $f(.,t) \subseteq \mathcal{T}^{m-1}$.

We will use this assumption in the remainder of the article. When f satisfies Assumption 2.1, for all $\ell \geq 0$, $\partial_t^\ell u(M_{m,j},0) = 0$, $j = 0,\ldots,p^m-1$, because of the finiteness of the wave propagation velocity.

2.4.1 Auxiliary notations

We will denote by $\boldsymbol{V}_\mu(\mathcal{T}^m)$ the following subspace of $\mathrm{H}^1_\mu(\mathcal{T}^m)$:

$$\boldsymbol{V}_\mu(\mathcal{T}^m) := \left\{ v \in \mathrm{H}^1_\mu(\mathcal{T}^m) : v(M^*) = 0 \right\}.$$

Let us introduce additionally the trace operator $\boldsymbol{\gamma}_m : \mathrm{H}^1_\mu(\mathcal{T}^m) \to \mathbb{R}^{p^m}$, defined for $v \in \mathrm{H}^1_\mu(\mathcal{T}^m)$ (recall that v is continuous on $\mathcal{T}^m$) by

$$\boldsymbol{\gamma}_m v = \Big(v(M_{m,0}), \ldots, v(M_{m,p^m-1}) \Big).$$

In the sequel, by $\langle .,. \rangle$ we will denote the Euclidean scalar product in $\mathbb{R}^{p^m}$. Obviously, by the usual trace theorem

$$\|\boldsymbol{\gamma}_m v\|_{\mathbb{R}^{p^m}} \leq C_{\gamma_m} \|\partial_s v\|_{\mathrm{H}^1_\mu(\mathcal{T}^m)}, \quad v \in \boldsymbol{V}_\mu(\mathcal{T}^m).$$

2.4.2 Transparent boundary conditions

Before describing the transparent BCs, let us introduce an auxiliary notation.

Remark 2.3 (Notation) In what follows, the notation ∂_t in $\mathcal{K}(\partial_t)$ indicates that the operator $\mathcal{K}(\partial_t)$ is a convolution operator. Namely, provided $g : \mathbb{R}^+ \to \mathbb{R}$, one has (with an abuse of notation, the integral below should be understood as a convolution of causal tempered distributions):

$$(\mathcal{K}(\partial_t)g)(t) = \int_0^t k(t-\tau)g(\tau)d\tau.$$

The Fourier–Laplace transform of the convolution kernel k, defined as

$$\boldsymbol{\mathcal{K}}(\omega) := (\mathcal{F}k)(\omega) = \int_0^\infty \mathrm{e}^{i\omega t} k(t)dt, \quad \omega \in \mathbb{C}^+,$$

will be denoted by $\boldsymbol{\mathcal{K}}$ (i.e. boldface $\mathcal{K}$) and referred to as the symbol of the operator $\mathcal{K}(\partial_t)$. Provided $\gamma > 0$, we will denote by $\mathcal{K}(\gamma\,\partial_t)$ a convolution operator with the symbol $\boldsymbol{\mathcal{K}}(\gamma\omega)$.

Transparent BCs We truncate the computational domain to the tree $\mathcal{T}^m$, and impose transparent boundary conditions at the (truncated) boundary of $\mathcal{T}^m$:

$$-\mu_{m,j}\,\partial_s u_{m,j}(M_{m,j},t) = \mathcal{B}^{\mathfrak{a}}_{m,j}(\partial_t)u_{m,j}(M_{m,j},t), \quad j=0,\dots,p^m-1, \tag{8}$$

where $\mathfrak{a}\in\{\mathfrak{d},\mathfrak{n}\}$ and $\mathcal{B}^{\mathfrak{a}}_{m,j}(\partial_t)$ is the exact DtN map for the Dirichlet (Neumann) problem, associated to the point $M_{m,j}$, that we describe below. Let

$$H^1_{0,loc}(\mathbb{R}^+) = \left\{ v\in H^1_{loc}(\mathbb{R}^+) :\ v(0)=0 \right\}.$$

Then this operator is a continuous mapping [30]:

$$\mathcal{B}^{\mathfrak{a}}_{m,j}(\partial_t) \in \mathcal{L}\left(H^1_{0,loc}(\mathbb{R}^+),\, L^2_{loc}(\mathbb{R}^+)\right).$$

To define this operator, let $\mathcal{T}_k := \mathcal{T}_{m,pj+k}$, $k=0,\dots,p-1$, are p-adic self-similar infinite subtrees of $\mathcal{T}$ sharing $M_{m,j}$ as the root vertex (cf. notation in the end of Sect. 2.1 and (1)). Because of the self-similarity property, see Sect. 2.1, the weights of their root edges are respectively $\mu_k\,\mu_{m,j}$, $k=0,\dots,p-1$. Then the DtN $\mathcal{B}^{\mathfrak{a}}_{m,j}(\partial_t)$ associates to $g\in H^1_{0,loc}(\mathbb{R}^+)$ the quantity

$$\mathcal{B}^{\mathfrak{a}}_{m,j}(\partial_t)g = -\sum_{k=0}^{p-1}\mu_{m,j}\,\mu_k\,\partial_s u^{\mathfrak{a}}_{g,k}(M_{m,j},\cdot), \tag{9}$$

where $u^{\mathfrak{a}}_{g,k}\in C^1(\mathbb{R}^+;\mathrm{L}^2_\mu(\mathcal{T}_k))$ is defined as follows:

1. if $\mathfrak{a}=\mathfrak{n}$, $u^{\mathfrak{n}}_{g,k}\in C(\mathbb{R}^+;\mathrm{H}^1_\mu(\mathcal{T}_k))$ solves the Neumann problem:

$$\begin{aligned} &\left(\partial_t^2 u^{\mathfrak{n}}_{g,k},\,v\right)_{\mathcal{T}_k} + \left(\partial_s u^{\mathfrak{n}}_{g,k},\,\partial_s v\right)_{\mathcal{T}_k} = 0, \quad \text{for all } v\in V_{\mathfrak{n}}(\mathcal{T}_k),\\ &u^{\mathfrak{n}}_{g,k}(M_{m,j},t) = g(t),\ u^{\mathfrak{n}}_{g,k}(.,0) = \partial_t u^{\mathfrak{n}}_{g,k}(.,0) = 0. \end{aligned} \tag{10}$$

2. if $\mathfrak{a}=\mathfrak{d}$, $u^{\mathfrak{d}}_{g,k}\in C(\mathbb{R}^+;\mathrm{H}^1_{\mu,0}(\mathcal{T}_k))$ solves (10) with $V_{\mathfrak{n}}$ replaced by $V_{\mathfrak{d}}$.

The definition (9) of the DtN map is obviously consistent with the Kirchoff conditions, cf. (8) and ($\mathcal{K}$). In a short form, we will write

$$\mathcal{B}^{\mathfrak{a}}_m(\partial_t) = \mathrm{diag}\left(\mathcal{B}^{\mathfrak{a}}_{m,0}(\partial_t),\dots,\mathcal{B}^{\mathfrak{a}}_{m,p^m-1}(\partial_t)\right). \tag{11}$$

With this notation, the transparent condition (8) rewrites

$$-\boldsymbol{\gamma}_m\big(\mu\,\partial_s u\big)(t) = \big(\mathcal{B}^{\mathfrak{a}}_m(\partial_t)u\big)(t). \tag{12}$$

Since the coefficients of the problem do not depend on time, $\mathcal{B}_m^{\mathfrak{a}}(\partial_t)$ is a convolution operator; the corresponding convolution kernel is not known in closed form. The goal of this work is to provide an accurate discrete approximation to $\mathcal{B}_m^{\mathfrak{a}}(\partial_t)$, which relies on a tractable characterization of its convolution kernel that was obtained in [33]. In order to show how to obtain an expression for $\mathcal{B}_m^{\mathfrak{a}}(\partial_t)$, let us first introduce the notion of the **reference** DtN operator.

2.4.3 Reference DtN operator

A reference DtN operator associated to the Dirichlet/Neumann problems on the **reference** tree $\mathcal{T}$ (i.e. the tree with $\ell_{0,0} = 1$) is defined as (see [30] for its mapping properties):

$$\begin{aligned} &\Lambda_{\mathfrak{a}}(\partial_t) \in \mathcal{L}\left(H^1_{0,loc}(\mathbb{R}^+),\ L^2_{loc}(\mathbb{R}^+)\right), \quad \mathfrak{a} \in \{\mathfrak{d}, \mathfrak{n}\}, \\ &\big(\Lambda_{\mathfrak{a}}(\partial_t) g\big)(t) = -\partial_s u_g^{\mathfrak{a}}(M^*, t), \quad g \in H^1_{0,loc}(\mathbb{R}^+), \end{aligned} \tag{13}$$

where $u_g^{\mathfrak{a}} \in C^1\big(\mathbb{R}^+; \mathrm{L}^2_\mu(\mathcal{T})\big)$ is defined as follows:

1. if $\mathfrak{a} = \mathfrak{n}$, $u_g^{\mathfrak{n}} \in C\big(\mathbb{R}^+; \mathrm{H}^1_\mu(\mathcal{T})\big)$ solves the Neumann problem:

$$\begin{aligned} &\left(\partial_t^2 u_g^{\mathfrak{n}}, v\right) + \left(\partial_s u_g^{\mathfrak{n}}, \partial_s v\right) = 0, \quad \text{for all } v \in V_{\mathfrak{n}}(\mathcal{T}), \\ &u_g^{\mathfrak{n}}(M^*, t) = g(t), \quad u_g^{\mathfrak{n}}(., 0) = \partial_t u_g^{\mathfrak{n}}(., 0) = 0. \end{aligned} \tag{14}$$

2. if $\mathfrak{a} = \mathfrak{d}$, $u_g^{\mathfrak{d}} \in C\big(\mathbb{R}^+; \mathrm{H}^1_{\mu,0}(\mathcal{T})\big)$ solves (14) with $V_{\mathfrak{n}}$ replaced by $V_{\mathfrak{d}}$.

Again, the operator $\Lambda_{\mathfrak{a}}(\partial_t)$ is a convolution operator, i.e. formally:

$$\Lambda_{\mathfrak{a}}(\partial_t) g(t) = \int_0^t \lambda_{\mathfrak{a}}(t-\tau) g(\tau) d\tau.$$

Following the notation introduced in Remark 2.3, we denote the symbol $(\mathcal{F}\lambda_{\mathfrak{a}})(\omega)$ of the convolution operator $\Lambda_{\mathfrak{a}}(\partial_t)$ by $\mathbf{\Lambda}_{\mathfrak{a}}(\omega)$.

Characterization and properties of $\mathbf{\Lambda}_{\mathfrak{a}}(\omega)$ A practical use of the CQ relies on the ability to compute the symbol of the DtN map, cf. (9), for various complex frequencies ω. In Sect. 2.4.4 we will show that this symbol can be easily expressed with the help of $\mathbf{\Lambda}_{\mathfrak{a}}(\omega)$. The latter function, in turn, satisfies the following non-linear equation, which will serve the computational purposes.

Lemma 2.1 (Lemma 5.3 in [33]) *The symbol of the reference DtN operator* $\mathbf{\Lambda}(\omega) = \mathbf{\Lambda}_{\mathfrak{a}}(\omega)$, $\mathfrak{a} \in \{\mathfrak{n}, \mathfrak{d}\}$, $\mathbf{\Lambda} : \mathbb{C}\backslash\mathbb{R} \to \mathbb{C}$, *satisfies the following equation:*

$$\mathbf{\Lambda}(\omega) = -\omega\, \frac{\omega \tan\omega - \mathbf{F}_{\alpha,\mu}(\omega)}{\tan\omega \mathbf{F}_{\alpha,\mu}(\omega) + \omega}, \quad \mathbf{F}_{\alpha,\mu}(\omega) = \sum_{i=0}^{p-1} \frac{\mu_i}{\alpha_i} \mathbf{\Lambda}(\alpha_i \omega). \tag{15}$$

Since the solutions of (15) are, in general, non-unique, to single out the solutions that correspond to the symbols of the DtN operators, we restrict the solution space to meromorphic even functions analytic in the origin, cf. Theorem 2.4. To distinguish between the solutions corresponding to the Dirichlet and Neumann problems (where needed, cf. Theorem 2.2), we fix the value $\mathbf{\Lambda}(0)$; this ensures the uniqueness. This is similar to initial-value problems, where fixing the value in zero leads to the uniqueness as well.

Theorem 2.3 (Lemma 5.5, Corollary 5.6, (144) in [33])

- *if* $\langle \boldsymbol{\mu}/\boldsymbol{\alpha} \rangle \leq 1$, *the symbol of the reference DtN operator* $\mathbf{\Lambda}_{\mathfrak{d}}(\omega) = \mathbf{\Lambda}_{\mathfrak{n}}(\omega)$ *is the unique even meromorphic solution of* (15) *that satisfies* $\mathbf{\Lambda}(0) = 0$.

- *let* $\langle \boldsymbol{\mu}/\boldsymbol{\alpha} \rangle > 1$ *and* $\langle \boldsymbol{\mu}\boldsymbol{\alpha} \rangle < 1$. *Then the function* $\mathbf{\Lambda}_{\mathfrak{d}}(\omega)$ *is the unique even meromorphic solution of* (15) *that satisfies* $\mathbf{\Lambda}(0) = 1 - 1/\langle \boldsymbol{\mu}/\boldsymbol{\alpha} \rangle$.
  Similarly, the function $\mathbf{\Lambda}_{\mathfrak{n}}(\omega)$ *is the unique even meromorphic solution of the Eq.* (15) *that satisfies* $\mathbf{\Lambda}(0) = 0$.

- *if* $\langle \boldsymbol{\mu}\boldsymbol{\alpha} \rangle \geq 1$, $\mathbf{\Lambda}_{\mathfrak{d}}(\omega) = \mathbf{\Lambda}_{\mathfrak{n}}(\omega)$ *is the unique even meromorphic solution of* (15) *that satisfies* $\mathbf{\Lambda}(0) = 1 - 1/\langle \boldsymbol{\mu}/\boldsymbol{\alpha} \rangle$.

The symbol $\mathbf{\Lambda}_{\mathfrak{a}}(\omega)$ satisfies the following property, which extends the well-known bounds for the DtN map for the classical wave equation on $\mathbb{R}^d$ [17].

Theorem 2.4 $\mathbf{\Lambda}_{\mathfrak{a}}(\omega) : \mathbb{C} \to \mathbb{C}$ *is an even meromorphic function, whose poles are all real. Moreover,*

(a) $\operatorname{Im}\left(\omega^{-1}\mathbf{\Lambda}_{\mathfrak{a}}(\omega)\right) < 0$ *for* $\omega \in \mathbb{C}^+ = \{z \in \mathbb{C} : \operatorname{Im} z > 0\}$.
(b) *There exists* $C > 0$, *s.t. for all* $\omega \in \mathbb{C}^+$, $|\mathbf{\Lambda}_{\mathfrak{a}}(\omega)| < C|\omega| \max\left(1, \frac{1}{\operatorname{Im}\omega}\right)$.

Proof The fact that $\mathbf{\Lambda}_{\mathfrak{a}}(\omega)$ is an even meromorphic function with real poles was shown in [33, Section 5.1]. The statement (a) is from Theorem 5.9 in [33]. The bound (b) is new and its proof is given in "Appendix A". □

Positivity of $\Lambda_{\mathfrak{a}}(\partial_t)$. The time-domain analogue of Theorem 2.4 (a) is the following (important) positivity result.

Theorem 2.5 *Let* $g \in H^1_{0,loc}(\mathbb{R}^+)$. *The reference DtN operator satisfies*

$$\int_0^T \left(\Lambda_{\mathfrak{a}}(\partial_t)g\right)(t)\, \partial_t g(t)\, dt \geq 0, \quad \mathfrak{a} \in \{\mathfrak{d}, \mathfrak{n}\}, \quad \text{for all } T > 0.$$

Proof The proof is classical. The result follows from an energy identity for (14), cf. the definition of $\Lambda_{\mathfrak{a}}(\partial_t)$. One finds that

$$\int_0^T \left(\Lambda_{\mathfrak{a}}(\partial_t)g\right)(t)\, \partial_t g(t)\, dt = \mathcal{E}^{\mathfrak{a}}_g(T) := \frac{1}{2}\left(\left\|\partial_t u^{\mathfrak{a}}_g(T)\right\|^2 + \left\|\partial_s u^{\mathfrak{a}}_g(T)\right\|^2\right).$$

□

2.4.4 Transparent boundary conditions via the reference DtN

Using the reference DtN, we can express the operator $\mathcal{B}^{\mathfrak{a}}_{m,j}(\partial_t)$ as follows [33]:

$$\mathcal{B}^{\mathfrak{a}}_{m,j}(\partial_t) = \mu_{m,j}\,\alpha^{-1}_{m,j} \sum_{k=0}^{p-1} \frac{\mu_k}{\alpha_k} \Lambda_{\mathfrak{a}}(\alpha_k \alpha_{m,j} \partial_t). \tag{16}$$

Recall that by $\Lambda_{\mathfrak{a}}(\alpha_k \alpha_{m,j} \partial_t)$ we denote a convolution operator with the symbol $\mathbf{\Lambda}_{\mathfrak{a}}(\alpha_k \alpha_{m,j} \omega)$, cf. Remark 2.3. The above representation was derived using the Kirchoff conditions and a scaling argument (recall in particular that $\alpha_{m,j}$ is the length of the branch $\Sigma_{m,j}$). We have thus reduced the problem of the construction of transparent boundary conditions to the problem of approximating a convolution operator with the symbol $\mathbf{\Lambda}_{\mathfrak{a}}(\omega)$.

Remark 2.4 Everything that follows, unless stated otherwise, holds true both for the Dirichlet and the Neumann problems, and the distinction between these two problems is encoded in the proper choice of the symbol $\mathbf{\Lambda}_{\mathfrak{a}}$. Hence, where possible, we will omit the index $\mathfrak{a} \in \{\mathfrak{d}, \mathfrak{n}\}$. We will study the Neumann problem, keeping in mind that the Dirichlet problem can be handled similarly.

2.4.5 Formulation on a truncated tree

With the notation from Sect. 2.4.1 and (11), the coupled problem with the transparent BCs reads, in the weak form:

$$\text{Find } u_m \in C\left(\mathbb{R}^+; \boldsymbol{V}_\mu(\mathcal{T}^m)\right) \cap C^1\left(\mathbb{R}^+; \mathrm{L}^2_\mu(\mathcal{T}^m)\right), \tag{17a}$$

$$\text{s.t. } u_m(.,0) = \partial_t u_m(.,0) = 0, \quad \text{and, for all } t > 0, \tag{17b}$$

$$\begin{aligned} &\left(\partial_t^2 u_m, v\right)_{\mathcal{T}^m} + (\partial_s u_m, \partial_s v)_{\mathcal{T}^m} + \left\langle \mathcal{B}_m(\partial_t) \boldsymbol{\gamma}_m u_m,\ \boldsymbol{\gamma}_m v \right\rangle \\ &\quad = (f, v)_{\mathcal{T}^m}, \quad \text{for all } v \in \boldsymbol{V}_\mu(\mathcal{T}^m). \end{aligned} \tag{17c}$$

We have the following easy-to-prove result.

Theorem 2.6 *For all $f \in L^1_{loc}(\mathbb{R}^+; \mathrm{L}^2_\mu(\mathcal{T}))$ satisfying Assumption 2.1, (17) has a unique solution u_m. Moreover, $u_m = u|_{\mathcal{T}^m}$, where u solves (N).*

Proof It is not difficult to verify that $u|_{\mathcal{T}^m} = u_m$ (by construction of the transparent condition via the operator $\mathcal{B}_m(\partial_t)$, cf. (9, 10)). This implies the existence for (17). The uniqueness follows easily from the energy identity

$$\frac{1}{2}\left(\|\partial_t u_m(T)\|^2_{\mathcal{T}^m} + \|\partial_s u_m(T)\|^2_{\mathcal{T}^m}\right) + \int_0^T \left\langle \mathcal{B}_m(\partial_t)\boldsymbol{\gamma}_m u_m,\ \boldsymbol{\gamma}_m \partial_t u_m \right\rangle dt = \int_0^T \int_{\mathcal{T}^m} \mu(s) f(s,t)\, u_m(s,t) ds\, dt. \tag{18}$$

If $f = 0$, (18), (16) and the positivity result of Theorem 2.5 imply $u_m = 0$. □

3 Discrete transparent boundary conditions (Convolution Quadrature (CQ))

The main idea behind the CQ is to construct the exact transparent boundary conditions for the problem (3) semi-discretized in time [3,45]. Provided that the time discretization scheme is chosen so that the resulting problem is stable, the corresponding exact transparent boundary conditions inherit its stability.

Remark 3.1 For the implementation of the convolution quadrature, it is important that the symbol of the operator $\mathcal{B}^{\mathfrak{a}}_{m,j}(\partial_t)$, i.e. $\boldsymbol{\mathcal{B}}^{\mathfrak{a}}_{m,j}(\omega)$ (consequently, $\boldsymbol{\Lambda}_{\mathfrak{a}}(\omega)$) can be evaluated for any frequency $\omega \in \mathbb{C}^+ = \{z \in \mathbb{C} : \operatorname{Im} z > 0\}$. The description of the respective method is postponed to Sect. 4, while here we address the questions of stability and convergence of the method.

This section is organized as follows:

- in Sect. 3.1 we derive discrete transparent boundary conditions based on the (implicit) trapezoid rule (also called θ-scheme with $\theta = \frac{1}{4}$);
- Section 3.2 is dedicated to the analysis of the semi-discretization in space;
- in Sect. 3.3 we provide the time discretization, demonstrate its stability and prove the convergence estimates;
- finally, Sect. 3.4 is dedicated to the solution of the discretized system.

3.1 Derivation of a CQ approximation for the transparent BCs

First, we will derive a discrete approximation for the reference DtN operator, see Sect. 2.4.3, and next employ the obtained results to derive an approximation for the transparent boundary conditions. Let Δt be a time step, $t^n = n\Delta t$. We denote by u^n

an approximation to $u(., t^n)$. Also,

$$\begin{aligned} D_{\Delta t} v^n &= \frac{v^{n+1} - v^{n-1}}{2\Delta t}, \quad D^2_{\Delta t} v^n = \frac{v^{n+1} - 2v^n + v^{n-1}}{(\Delta t)^2}, \\ \{v^n\}_{1/4} &= \frac{v^{n+1} + 2v^n + v^{n-1}}{4}, \quad v^{n+1/2} = \frac{v^n + v^{n+1}}{2}, \\ D_{\Delta t} v^{n+1/2} &= \frac{v^{n+1} - v^n}{\Delta t}. \end{aligned} \tag{19}$$

3.1.1 Discrete approximation of $\Lambda(\partial_t)$

To derive the CQ approximation of $\Lambda(\partial_t)$, we will proceed like in the continuous case, see Sect. 2.4.3. We start with the problem (14), which we semi-discretize in time using the trapezoid rule (θ-scheme with $\theta = \frac{1}{4}$). As well-known [14], this scheme is unconditionally stable, and thus the discretization results in a well-posed and stable problem. Recall that our goal is to approximate the transparent boundary conditions (8), cf. (16); because of the finite velocity of the wave propagation, $u_m(M_{m,j}, .)$ vanishes in the vicinity of $t = 0$ (cf. Assumption 2.1); therefore, without loss of generality in what follows we assume that $g(0) = g'(0) = g''(0) = 0$. The discretized problem then reads:

$$\begin{aligned} &\text{Given } u_g^0 = 0, u_g^1 = 0,\ u_g^n(M^*) = g^n, \quad \text{find } \left(u_g^n\right)_{n\in\mathbb{N}} \subset \mathrm{H}^1_\mu(\mathcal{T}), \text{ s.t.} \\ &\left(D^2_{\Delta t} u_g^n, v\right) + \left(\partial_s \left\{u_g^n\right\}_{1/4}, \partial_s v\right) = 0, \quad \text{for all } v \in V_{\mathfrak{n}}, \quad n \geq 1. \end{aligned} \tag{20}$$

The reference DtN is then defined analogously to the continuous case (13), $\Lambda(\partial_t^{\Delta t}) : \mathbb{R}^{\mathbb{N}} \to \mathbb{R}^{\mathbb{N}}$ and, with $\boldsymbol{g} = (g^n)_{n\in\mathbb{N}}$,

$$\left(\Lambda\left(\partial_t^{\Delta t}\right)\boldsymbol{g}\right)^n = -\partial_s u_g^n(M^*), \quad n \geq 0. \tag{21}$$

Where convenient, we will write instead of the above $\Lambda(\partial_t^{\Delta t}) g^n$, with the obvious abuse of notation. In the above form, the reference DtN operator is not suitable for the computations; thus, let us find a tractable expression for its discrete symbol. For this we will use the Z-transform.

The symbol of the discrete DtN operator Let us apply the Z-transform to the above problem. Recall that for a sequence $(v^n)_{n\in\mathbb{N}}$, s.t. $|v^n| < C(1+n)^q$, $q \geq 0$, its Z-transform is defined as follows:

$$Z : v = (v^n)_{n\in\mathbb{N}} \mapsto V(z) = \sum_{n=0}^{\infty} v^n z^n, \quad z \in B_1(0) = \{z \in \mathbb{C} : |z| < 1\}. \tag{22}$$

The function V is obviously analytic in $B_1(0)$. Applying the Z-transform to (20), and using the following property of the Z-transform of the shift τ:

$$\text{for } v = (0, v_1, v_2, \ldots), \quad \tau v := (v_1, v_2, \ldots) \quad \text{and} \quad Z(\tau v) = z^{-1} V(z), \tag{23}$$

we deduce that $U_g(z) \in \mathrm{H}^1_\mu(\mathcal{T})$ satisfies $U_g(M^*, z) = G(z)$ and

$$-\left(i\frac{\delta(z)}{\Delta t}\right)^2 \big(U_g, v\big) + \big(\partial_s U_g, \partial_s v\big) = 0, \quad \forall\, v \in V_{\mathfrak{n}}, \quad \delta(z) = 2\,\frac{1-z}{1+z}. \tag{24}$$

Since $i\delta : B_1(0) \to \mathbb{C}^+ = \{\omega \in \mathbb{C} : \operatorname{Im}\omega > 0\}$, the problem (24) is coercive for any $z \in B_1(0)$. With the help of (24), we can then define the discrete symbol of the reference DtN as the mapping

$$\mathbf{\Lambda}_{\Delta t} : \mathbb{C} \to \mathbb{C}, \quad \mathbf{\Lambda}_{\Delta t}(z) : G(M^*, z) \to -\partial_s U_g(M^*, z). \tag{25}$$

Comparing (24) and the definition of the symbol $\mathbf{\Lambda}(\omega)$, we obtain

$$\mathbf{\Lambda}_{\Delta t}(z) \equiv \mathbf{\Lambda}\left(i\frac{\delta(z)}{\Delta t}\right). \tag{26}$$

Because $\mathbf{\Lambda}(\omega)$ is analytic in $\mathbb{C}^+ := \{\omega \in \mathbb{C} : \operatorname{Im}\omega > 0\}$, cf. Theorem 2.4, and $z \mapsto \frac{i\delta(z)}{\Delta t}$ is an analytic function from $B_1(0)$ into $\mathbb{C}^+$, we conclude that $\mathbf{\Lambda}_{\Delta t}(z)$ is analytic inside $B_1(0)$. Thus, $\mathbf{\Lambda}_{\Delta t}$ can be expressed via its Laurent series

$$\mathbf{\Lambda}_{\Delta t}(z) = \sum_{\ell=0}^{\infty} \lambda_\ell^{\Delta t} z^\ell, \quad |z| < 1. \tag{27}$$

The coefficients $\lambda_\ell^{\Delta t}$ are called convolution weights. Alternatively, they can be represented via the Cauchy integrals (with γ being a directly oriented circle of radius $r < 1$ centered at the origin):

$$\lambda_\ell^{\Delta t} = \frac{1}{2\pi i}\int_\gamma z^{-\ell-1}\mathbf{\Lambda}_{\Delta t}(z)\,dz = \frac{1}{2\pi i}\int_\gamma z^{-\ell-1}\mathbf{\Lambda}\left(i\frac{\delta(z)}{\Delta t}\right)dz. \tag{28}$$

$\Lambda(\partial_t^{\Delta t})$ as a convolution operator Inverting the Z-transform in (25), using (27) and the property (23), we obtain the discretization of the reference DtN:

$$-\partial_s u_g^n(M^*) = \sum_{\ell=0}^{n} \lambda_\ell^{\Delta t} g^{n-\ell} =: \Lambda\left(\partial_t^{\Delta t}\right) g^n. \tag{29}$$

In what follows, provided a convolution operator with the symbol $\mathcal{K}(\omega)$ (and the respective discrete symbol $\mathcal{K}\big(i\,\delta(z)/\Delta t\big)$), we will use the notation $\mathcal{K}(\partial_t^{\Delta t})g^n$ to denote

the discrete convolution of the discretized operator and the sequence $(g^n)_{n\in\mathbb{N}}$ (cf. Remark 2.3 for the continuous case). To compute the convolution (29), it is sufficient to know the convolution weights $\lambda_\ell^{\Delta t}$; classically [38], their evaluation is done based on the fast numerical computation of the Cauchy integrals (28), see Sect. 4.1.

Positivity properties of $\Lambda(\partial_t^{\Delta t})$ The following result, which we state here for consistency reasons, is a discrete counterpart of Theorem 2.5.

Theorem 3.1 *Let* $(g^n)_{n\in\mathbb{N}} \in \mathbb{R}^{\mathbb{N}}$, *with* $g^0 = g^1 = 0$. *Then, for all* $N \geq 2$,

$$\sum_{n=1}^{N-1} \left\{ \Lambda\left(\partial_t^{\Delta t}\right) g^n \right\}_{1/4} D_{\Delta t} g^n \geq 0.$$

Proof The proof mimics the proof of Theorem 2.5, namely, the result is obtained by testing the strong form of (20) with $D_{\Delta t} u_g^n$. In particular one finds

$$\sum_{n=1}^{N-1} \left\{ \Lambda\left(\partial_t^{\Delta t}\right) g^n \right\}_{1/4} D_{\Delta t} g^n = \frac{1}{2} \left(\left\| D_{\Delta t} u_g^{N-\frac{1}{2}} \right\|^2_{\mathrm{L}^2_\mu(\mathcal{T})} + \left\| \partial_s u_g^{N-\frac{1}{2}} \right\|^2_{\mathrm{L}^2_\mu(\mathcal{T})} \right).$$

□

3.1.2 Discrete approximation of the operators $\mathcal{B}_{m,j}(\partial_t)$

To derive a discrete approximation of $\mathcal{B}_{m,j}(\partial_t)$, we follow the same arguments as in the continuous case, cf. Sects. 2.4.2 and 2.4.4. This yields the following discrete counterpart of (16), cf. (21) for the definition of $\Lambda(\partial_t^{\Delta t})$:

$$\mathcal{B}_{m,j}\left(\partial_t^{\Delta t}\right) = \mu_{m,j}\, \alpha_{m,j}^{-1} \sum_{k=0}^{p-1} \frac{\mu_k}{\alpha_k} \Lambda\left(\alpha_{m,j}\alpha_k \partial_t^{\Delta t}\right), \tag{30}$$

which is a discrete convolution operator with the symbol

$$\boldsymbol{\mathcal{B}}_{m,j}^{\Delta t}(z) = \mu_{m,j}\, \alpha_{m,j}^{-1} \sum_{k=0}^{p-1} \frac{\mu_k}{\alpha_k} \boldsymbol{\Lambda}\left(i\alpha_{m,j}\alpha_k \frac{\delta(z)}{\Delta t}\right), \tag{31}$$

cf. (26). As a consequence, the convolution weights $\left(b_{m,j;n}^{\Delta t}\right)$ of $\boldsymbol{\mathcal{B}}_{m,j}^{\Delta t}(z)$ are related to the convolution weights $\left(\lambda_n^{\Delta t}\right)$ via the identity

$$b_{m,j;n}^{\Delta t} = \mu_{m,j}\, \alpha_{m,j}^{-1} \sum_{k=0}^{p-1} \frac{\mu_k}{\alpha_k} \lambda_n^{\Delta t_{m,j;k}}, \quad \Delta t_{m,j;k} = \frac{\Delta t}{\alpha_{m,j}\, \alpha_k}. \tag{32}$$

Finally, let us introduce the notation for the discrete version of the aggregate operator $\mathcal{B}_m(\partial_t)$, cf. (11): its discretization will be denoted by $\mathcal{B}_m(\partial_t^{\Delta t})$, the corresponding

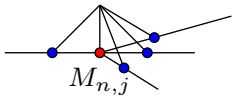

Fig. 2 A shape function φ s.t. $\varphi(M_{n,j}) = 1$

symbol by $\boldsymbol{\mathcal{B}}_m^{\Delta t}(z)$, and the respective convolution weights by $\boldsymbol{b}_{m,n}^{\Delta t}$ (remark that they are $m \times m$ diagonal matrices).

3.2 Semi-discretization in space

3.2.1 Semi-discretization in space: basics

To semi-discretize the system (17) in space, we use the Lagrange $\mathbb{P}_1$-elements. Let us parametrize each edge $\Sigma_{n,j}$, identified with a segment $[M_{n,j}^*,\ M_{n,j}]$, with an abscissa $s_{n,j} \in [0,\ell_{n,j}]$, and define a quasi-uniform mesh

$$T_{n,j} = \left\{ s_{n,j}^k,\quad k = 0,\dots,K_{n,j} \right\},\quad \text{s.t. } s_{n,j}^k < s_{n,j}^{k+1}, \tag{33}$$

where $s_{n,j}^0$ is identified with $M_{n,j}^*$, and $s_{n,j}^{K_{n,j}}$ with $M_{n,j}$.

The mesh on the truncated tree $\mathcal{T}^m$ is then $\bigcup_{n=0}^m \bigcup_{j=0}^{p^n-1} T_{n,j}$. Let

$$h_{n,j} := \max_{1\le k\le K_{n,j}} \left| s_{n,j}^k - s_{n,j}^{k-1} \right|,\quad h := \max_n \max_j h_{n,j}. \tag{34}$$

Let the finite element space be defined as $U_h \subset \boldsymbol{V}_\mu(\mathcal{T}^m)$, $U_h = \text{span}\{\varphi_k,\ k = 0,\dots,N_s-1\}$. The construction of this basis is classical on the nodes interior to $\Sigma_{n,j}$, but a special treatment is needed in the vertices of the graph $M_{n,j}$, see [1]: we define the respective shape function as a piecewise-linear function that equals to 1 in $M_{n,j}$ and vanishes in the rest of the nodes, see Fig. 2.

In the following, $u_h = \sum u_{(k)}\varphi_k$ will denote the approximation to the exact solution u_m, $u_{(k)}$ being a nodal value. For convenience we omit the index m.

3.2.2 Semi-discrete system: formulation and stability

The semi-discrete formulation of (17) with the exact transparent boundary conditions thus reads:

$$\begin{aligned} &\text{Find } u_h \in C^1(\mathbb{R}^+; U_h),\ \text{s.t. } u_h(0) = \partial_t u_h(0) = 0,\ \text{and, for all } v_h \in U_h,\\ &\left(\partial_t^2 u_h,\, v_h\right)_{\mathcal{T}^m} + (\partial_s u_h,\, \partial_s v_h)_{\mathcal{T}^m} + \langle \mathcal{B}_m(\partial_t)\boldsymbol{\gamma}_m u_h,\ \boldsymbol{\gamma}_m v_h\rangle = (f,\, v_h)_{\mathcal{T}^m}. \end{aligned} \tag{35}$$

The stability of the above problem follows trivially using the argument of Theorem 2.6; however, the existence of a solution is somewhat more difficult. For analysis purposes, we will rewrite the above problem in a different form.

Rewriting of (35) The idea is to propose an auxiliary semi-discrete problem, set on the whole tree $\mathcal{T}$, whose restriction to $\mathcal{T}^m$ solves (35).

Let us introduce the following two Hilbert spaces:

$$L^h := \left\{ v_h \in \mathrm{L}^2_\mu(\mathcal{T}) : \ v_h|_{\mathcal{T}^m} \in U_h \right\}, \quad \|.\|_{L^h} := \|.\|_{\mathrm{L}^2_\mu},$$
$$X^h := \{ v_h \in V_{\mathfrak{n}}(\mathcal{T}) : \ v_h|_{\mathcal{T}^m} \in U_h \}, \quad \|.\|_{X^h} := \|.\|_{\mathrm{H}^1_\mu}. \tag{36}$$

Contrary to the space U_h, these spaces are infinite-dimensional, the reason why we use h as a superscript. In particular, the restriction of functions from X^h to each $\mathcal{T}_{m+1,pj+k}$, $j = 0, \ldots, p^m$, $k = 0, \ldots, p-1$ (see the end of Sect. 2.1 and (1) for the notation) coincides with the space $\mathrm{H}^1_\mu(\mathcal{T}_{m+1,pj+k})$ (recall that we consider the Neumann problem).

Let us now study the following auxiliary problem (a counterpart of (35)):

$$\text{find } \bar{u}_h \in C(\mathbb{R}^+; X^h) \cap C^1(\mathbb{R}^+; L^h), \text{ s.t. } \bar{u}_h(0) = \partial_t \bar{u}_h(0) = 0, \text{ and}$$
$$\left(\partial_t^2 \bar{u}_h, v_h\right) + (\partial_s \bar{u}_h, \partial_s v_h) = (f, v_h), \quad \text{for all } v_h \in X^h. \tag{37}$$

Using the above auxiliary problem, it will be easy to show the well-posedness and stability of (35). This approach to the analysis of the coupled problem bears some similarities with [24,41], see also references therein.

Well-posedness and stability of (35) We proceed as follows: first, in Lemma 3.1 we show the well-posedness/stability of (37), next, in Lemma 3.2 argue that $\bar{u}^n|_{\mathcal{T}^m}$ solves (35). Finally, a complete well-posedness/stability result for (35) is summarized in Theorem 3.2.

Lemma 3.1 [Well-posedness, stability of (37)] *For any source term $f \in L^1_{loc}(\mathbb{R}^+; \mathrm{L}^2_\mu(\mathcal{T}))$, the problem (37) has a unique solution. Moreover, it satisfies the stability bound (6) with u replaced by $\bar{u}_h$.*

Proof The existence and uniqueness to (37) follows from the semigroup theory. In particular, let us introduce the operator $A_h : D(A_h) \to L^h$ defined for $v_h, w_h \in X^h$ by $(A_h v_h, w_h) = a(v_h, w_h) := (\nabla v_h, \nabla w_h)$. Here

$$D(A_h) = \left\{ v_h \in X^h : \exists\, C(v_h) > 0,\ |a(v_h, w_h)| \le C(v_h)\, \|w_h\|_{L^h},\ \forall\, w_h \in X^h \right\}.$$

Then the problem (37) can be reformulated as an abstract wave equation

$$\frac{d^2}{dt^2} \bar{u}_h + A_h \bar{u}_h = \Pi^h f,$$

where Π^h is the L^2_μ-orthogonal projector on L^h. We conclude using the same arguments as in the proof of Theorem 2.1. The stability bound also follows like in the proof of Theorem 2.1. □

In the following we state that the solution of (37) solves (35).

Lemma 3.2 *Let $f \in L^1_{loc}(\mathbb{R}^+; \mathrm{L}^2_\mu(\mathcal{T}))$ satisfy Assumption 2.1, and let $\bar{u}_h$ solve (37). Then, the restriction of $\bar{u}_h$ to $\mathcal{T}^m$ is the solution u_h of (35).*

Proof We can split the variational formulation in (37) into two parts:

$$\begin{aligned}&\left(\partial_t^2 \bar{u}_h, v_h\right)_{\mathcal{T}^m} + (\partial_s \bar{u}_h, \partial_s v_h)_{\mathcal{T}^m} \\ &\quad + \left(\partial_t^2 \bar{u}_h, v_h\right)_{\mathcal{T}\setminus\mathcal{T}^m} + (\partial_s \bar{u}_h, \partial_s v_h)_{\mathcal{T}\setminus\mathcal{T}^m} = (f, v_h)_{\mathcal{T}^m}, \quad \forall v_h \in X^h.\end{aligned} \tag{38}$$

Taking the test functions v_h vanishing in $\mathcal{T}^m$, we deduce that

$$\begin{aligned}&\left(\partial_t^2 \bar{u}_h, v_h\right)_{\mathcal{T}\setminus\mathcal{T}^m} + (\partial_s \bar{u}_h, \partial_s v_h)_{\mathcal{T}\setminus\mathcal{T}^m} = 0, \\ &\quad \text{for all } v_h \in \mathrm{H}^1_\mu(\mathcal{T}\setminus\mathcal{T}^m), \text{ s.t. } v_h(M_{m,j}) = 0, \ j = 0, \dots, p^m - 1,\end{aligned}$$

i.e. (10) with $g(t) \equiv \bar{u}_h(M_{m,j}, t)$. Integrating by parts the two last terms in the r.h.s. of (38) and using the definition of the transparent BCs (9), we conclude that $\bar{u}_h \in X^h$ satisfies: for all $v_h \in X^h$,

$$\left(\partial_t^2 \bar{u}_h, v_h\right)_{\mathcal{T}^m} + (\partial_s \bar{u}_h, \partial_s v_h)_{\mathcal{T}^m} + \langle \mathcal{B}_m(\partial_t) \boldsymbol{\gamma}_m \bar{u}_h, \boldsymbol{\gamma}_m v_h \rangle = (f, v_h)_{\mathcal{T}^m}. \tag{39}$$

Since $X^h\big|_{\mathcal{T}^m} \equiv U_h$, we deduce that $\bar{u}_h|_{\mathcal{T}^m}$ solves (35). □

The following theorem is a simple corollary of the two above results.

Theorem 3.2 [Well-posedness, stability of (35)] *The problem (35) has a unique solution for any $f \in L^1_{loc}(\mathbb{R}^+; \mathrm{L}^2_\mu(\mathcal{T}^m))$. Also, there exists $C > 0$ s.t., for all $T > 0$, $0 \le t \le T$,*

$$\|\partial_t u_h(t)\|_{\mathcal{T}^m} + \|\partial_s u_h(t)\|_{\mathcal{T}^m} \le C \|f\|_{L^1\left(0,T;\mathrm{L}^2_\mu(\mathcal{T}^m)\right)}. \tag{40}$$

Proof Existence: by Lemma 3.1, there exists a unique $\bar{u}_h$ solving (35); by Lemma 3.2, $\bar{u}_h|_{\mathcal{T}^m} \in U_h$ satisfies (37). The uniqueness is a corollary of (40), which, in turn, follows from the same argument as in Theorem 2.6. □

3.2.3 Convergence estimates for the spatial semi-discretization

In this section we will compare u_m solving (17) to u_h solving (35). The proofs presented below use classical techniques of the FEM convergence for time-dependent problems, see e.g. [29] and references therein, or the monograph [18, Chapter 6]. The difference between our case and these works lies in the fact that we analyze the problem (37), posed on an infinite-dimensional, rather than FEM, space. We shall make the following

regularity assumption on f (the assumption of vanishing derivatives at $t = 0$ is not necessary but allows us to simplify the obtained estimates):

$$f \in W^{3,1}_{loc}\left(\mathbb{R}^+; \mathrm{L}^2_\mu(\mathcal{T}^m)\right), \quad \partial_t^\ell f(.,0) = 0, \ 0 \le \ell \le 2. \tag{41}$$

Theorem 3.3 (Convergence of the spatial discretization) *Assume* (41). *Let* u_h *solve* (35), *and* u_m *solve* (17). *Then, for all* $T > 0$, *with* $C_T = C\max(1, T)$, $C > 0$, *it holds, for all* $0 \le t \le T$,

$$\|\partial_t(u_m - u_h)(t)\|_{\mathrm{L}^2_\mu(\mathcal{T}^m)} + \|\partial_s(u_m - u_h)(t)\|_{\mathrm{L}^2_\mu(\mathcal{T}^m)} \le C_T h \|f\|_{W^{3,1}\left(0,T;\mathrm{L}^2_\mu(\mathcal{T}^m)\right)}.$$

We will prove this result by comparing the solution u of (N) to the solution $\bar{u}_h$ of (37), which is justified by Theorem 2.6 and Lemma 3.2. Obviously,

$$\begin{aligned} &\|\partial_t(u_m - u_h)\|_{\mathrm{L}^2_\mu(\mathcal{T}^m)} + \|\partial_s(u_m - u_h)\|_{\mathrm{L}^2_\mu(\mathcal{T}^m)} \\ &\quad \le \|\partial_t(u - \bar{u}_h)\|_{\mathrm{L}^2_\mu(\mathcal{T}^m)} + \|\partial_s(u - \bar{u}_h)\|_{\mathrm{L}^2_\mu(\mathcal{T}^m)}. \end{aligned} \tag{42}$$

The proof itself is quite classical. Let us introduce an elliptic projection operator $P^h : V_{\mathfrak{n}}(\mathcal{T}) \to X^h$ defined for $v \in V_{\mathfrak{n}}(\mathcal{T})$ via

$$\left(v - P^h v, v_h\right)_{\mathcal{T}} + \left(\partial_s\left(v - P^h v\right), \partial_s v_h\right)_{\mathcal{T}} = 0, \quad \text{for all } v_h \in X^h. \tag{43}$$

To analyze the convergence, we split the error into two parts:

$$u - \bar{u}_h = \eta_h + \varepsilon_h, \quad \eta_h = u - P^h u, \quad \varepsilon_h = P^h u - \bar{u}_h, \tag{44}$$

and estimate ε_h in terms of η_h (which, in turn, will be shown to be small), via the energy techniques. Let us first provide lemmas that quantify η_h.

Estimates on the projection error Let us introduce the space

$$\widetilde{H}^2_\mu(\mathcal{T}^m) := \left\{ v \in \mathrm{H}^1_\mu(\mathcal{T}^m) : \ \partial_s^2 v\Big|_{\Sigma_{\ell,j}} \in L^2(\Sigma_{\ell,j}), \ 0 \le \ell \le m, \ 0 \le j \le p^\ell - 1 \right\},$$

$$\|v\|^2_{\widetilde{H}^2_\mu(\mathcal{T}^m)} = \|v\|^2_{\mathrm{H}^1_\mu(\mathcal{T}^m)} + |v|^2_{\widetilde{H}^2_\mu(\mathcal{T}^m)}, \quad |v|^2_{\widetilde{H}^2_\mu(\mathcal{T}^m)} := \sum_{\ell=0}^{m} \sum_{j=0}^{p^\ell - 1} \mu_{\ell,j} \int_{\Sigma_{\ell,j}} \left|\partial_s^2 v\right|^2 ds.$$

The following is a usual approximation result extended to X^h. The proof, based on Céa's lemma, is left to the reader.

Lemma 3.3 *For* $v \in V_{\mathfrak{n}}(\mathcal{T})$, *s.t.* $v|_{\mathcal{T}^m} \in \widetilde{H}^2_\mu(\mathcal{T}^m)$, *it holds*

$$\|v - P_h v\|_{\mathrm{L}^2_\mu(\mathcal{T})} + \|\partial_s(v - P_h v)\|_{\mathrm{L}^2_\mu(\mathcal{T})} \le C\, h\, |v|_{\widetilde{H}^2_\mu(\mathcal{T}^m)},$$

where C depends on p, m only.

As a corollary of this result, we obtain the following.

Lemma 3.4 (Estimate for $\|\partial_t^k \eta_h\|$) *Let f satisfy (41). Let u solve (N) and η_h be defined in (44). Then, there exists $C > 0$, s.t. for all $T > 0$, $0 \le t \le T$, and all $0 \le \ell \le 2$,*

$$\left\|\partial_t^\ell \eta_h(t)\right\|_{\mathrm{H}^1_\mu(\mathcal{T})} \le Ch \left\|\partial_t^{\ell+1} f\right\|_{L^1\left(0,T;\mathrm{L}^2_\mu(\mathcal{T})\right)}. \tag{45}$$

Proof By Corollary 2.1, $u \in C^4(\mathbb{R}^+; \mathrm{L}^2_\mu(\mathcal{T}))$. By Lemma 3.3, for $v = \partial_t^\ell u$,

$$\left\|\partial_t^\ell \eta_h(t)\right\|_{\mathrm{H}^1_\mu(\mathcal{T})} \le Ch \left|\partial_t^\ell u(t)\right|_{\widetilde{H}^2_\mu(\mathcal{T}^m)}. \tag{46}$$

Let us prove that the right-hand side is bounded and provide an explicit bound for it. Since on all edges $\Sigma_{\ell,j}$, it holds that $\partial_s^2 u = \partial_t^2 u - f$, we have

$$\left|\partial_t^\ell u(t)\right|_{\widetilde{H}^2_\mu(\mathcal{T}^m)} \le \left\|\partial_t^{2+\ell} u(t)\right\|_{\mathrm{L}^2_\mu(\mathcal{T}^m)} + \left\|\partial_t^\ell f(t)\right\|_{\mathrm{L}^2_\mu(\mathcal{T}^m)}.$$

One concludes using (46), (7) and $\|\partial_t^\ell f(t)\|_{\mathrm{L}^2_\mu(\mathcal{T}^m)} \le \int_0^t \left\|\partial_t^{\ell+1} f(\tau)\right\|_{\mathrm{L}^2_\mu(\mathcal{T}^m)} d\tau$. □

Proof of Theorem 3.3 As discussed, see (42), we will compare the solution u of (N) to $\bar{u}_h$ from (37). With (44), we can see that $\varepsilon_h \in X^h$ satisfies

$$\left(\partial_t^2 \varepsilon_h, v_h\right) + (\partial_s \varepsilon_h, \partial_s v_h) = -\left(\partial_t^2 \eta_h, v_h\right) - (\partial_s \eta_h, \partial_s v_h), \quad v_h \in X^h.$$

By (43) and the definition of η_h in (44),

$$\left(\partial_t^2 \varepsilon_h, v_h\right) + (\partial_s \varepsilon_h, \partial_s v_h) = -\left(\partial_t^2 \eta_h, v_h\right) + (\eta_h, v_h), \quad v_h \in X^h.$$

By Lemma 3.1, the bound (6) applies to ε_h defined as above; thus, for all $T \ge 0$ and all $0 \le t \le T$,

$$\begin{aligned}\|\partial_t \varepsilon_h(t)\| + \|\partial_s \varepsilon_h(t)\| &\le C \int_0^T \left(\left\|\partial_t^2 \eta_h(\tau)\right\|_{\mathrm{L}^2_\mu(\mathcal{T})} + \|\eta_h(\tau)\|_{\mathrm{L}^2_\mu(\mathcal{T})}\right) dt \\ &\le \tilde{C}\, h\, T \int_0^T \left(\left\|\partial_t^3 f(\tau)\right\|_{\mathrm{L}^2_\mu(\mathcal{T}^m)} + \|\partial_t f(\tau)\|_{\mathrm{L}^2_\mu(\mathcal{T}^m)}\right) dt,\end{aligned}$$

where the last inequality follows from (45). Combining the above bound with the triangle inequality, i.e.

$$\|\partial_t(u - \bar{u}_h)\| + \|\partial_s(u - \bar{u}_h)\| \le \|\partial_t \eta_h\| + \|\partial_s \eta_h\| + \|\partial_t \varepsilon_h\| + \|\partial_s \varepsilon_h\|,$$

and using (45) to bound the first two terms in the right hand side, we obtain the desired result in the statement of the theorem. □

Remark 3.2 Obviously, the convergence is only $O(h)$ because we measure the error in the energy norm; using the Aubin–Nitsche techniques, we can deduce the convergence $O(h^2)$ when measuring $\|u_m - u_h\|_{\mathrm{L}^2_\mu(\mathcal{T}^m)}$.

3.3 Fully discrete problem

For the time discretization of the semi-discrete problem (35), we wish to use the leap-frog scheme, at least for the first two terms of the left hand side of (35). An advantage is that, if a mass lumping procedure is applied [15], the scheme becomes fully explicit. Moreover, if one uses a uniform space step h for meshing $\mathcal{T}^m$, and the time step Δt equals h, the scheme becomes exact.

In what follows, for simplicity, we shall not consider mass lumping in our analysis, but this analysis could be easily extended to the mass lumped case. The main issue is the approximation of the boundary term in (35). This is where the discrete operators $\mathcal{B}_m(\partial_t^{\Delta t})$ will be involved. In order to guarantee the stability of the resulting scheme, we will use the equivalence between (35) and (37) and discretize (37) in time in a specific way.

3.3.1 Construction of the numerical scheme

In what follows we denote by u_h^n (resp. $\bar{u}_h^n$) a discrete approximation to $u_h(t^n)$ (resp. $\bar{u}_h(t^n)$). To discretize (35), we start with the split variational formulation (38). The key point is that we use an explicit/implicit time discretization of the stiffness bilinear form: we use $(\partial_s \bar{u}_h^n, \partial_s v)_{\mathcal{T}^m}$ for approximating $(\partial_s \bar{u}_h(t^n), \partial_s v)_{\mathcal{T}^m}$ (thus obtaining the leapfrog discretization) and the θ-scheme with $\theta = \frac{1}{4}$, namely $(\partial_s \{\bar{u}_h^n\}_{1/4}, \partial_s v)_{\mathcal{T}\setminus\mathcal{T}^m}$, for approximating the remaining term $(\partial_s \bar{u}_h(t^n), \partial_s v)_{\mathcal{T}\setminus\mathcal{T}^m}$. The resulting scheme reads:

$$\begin{aligned}&\left(D^2_{\Delta t}\bar{u}_h^n, v_h\right)_{\mathcal{T}^m} + \left(\partial_s \bar{u}_h^n, \partial_s v_h\right)_{\mathcal{T}^m}\\ &\quad + \left(D^2_{\Delta t}\bar{u}_h^n, v_h\right)_{\mathcal{T}\setminus\mathcal{T}^m} + \left(\partial_s\left\{\bar{u}_h^n\right\}_{1/4}, \partial_s v_h\right)_{\mathcal{T}\setminus\mathcal{T}^m} = (f^n, v_h)_{\mathcal{T}^m},\ \forall v_h \in X^h.\end{aligned} \tag{47}$$

According to Lemma 3.2, it is natural to define u_h^n as the restriction to $\mathcal{T}^m$ of $\bar{u}_h^n$ (assuming it exists, it will be shown in Lemma 3.5). Proceeding like in the proof of Lemma 3.2, and using the definition of the operators $\mathcal{B}_m(\partial_t^{\Delta t})$, Sect. 3.1.2, it is easy to see that $u_h^n \in U_h$ satisfies

$$\begin{aligned}&\left(D^2_{\Delta t}u_h^n, v_h\right)_{\mathcal{T}^m} + \left(\partial_s u_h^n, \partial_s v_h\right)_{\mathcal{T}^m}\\ &\quad + \left\langle\left\{\mathcal{B}_m\left(\partial_t^{\Delta t}\right)\boldsymbol{\gamma}_m u_h^n\right\}_{1/4}, \boldsymbol{\gamma}_m v_h\right\rangle = (f^n, v_h)_{\mathcal{T}^m},\quad \forall\, v_h \in U_h,\end{aligned} \tag{48}$$

which, assuming also that $f(.,0) = \partial_t f(.,0) = 0$, we complete with

$$u_h^0 = 0, \quad u_h^1 = 0. \tag{49}$$

Remark 3.3 Reinterpreting (48), we see that the discrete transparent condition issued from (48) (to be compared with the continuous one (12)) reads

$$-\boldsymbol{\gamma}_m\left(\mu\,\partial_s u_h^n\right) = \left\{\mathcal{B}_m\left(\partial_t^{\Delta t}\right)\boldsymbol{\gamma}_m u_h^n\right\}_{1/4}, \tag{50}$$

which is not a priori the most natural (or naive) idea.

3.3.2 Well-posedness and stability of the fully discrete problem (48, 49).

This section dedicated to the proof of the well-posedness and stability of (48, 49) under the following CFL condition

$$C_{cfl}^2 = \frac{\Delta t^2}{4} \sup_{v_h \in U_h : \|v_h\|_{\mathrm{L}^2_\mu(\mathcal{T}^m)}=1} \|\partial_s v_h\|^2_{\mathrm{L}^2_\mu(\mathcal{T}^m)} < 1. \tag{51}$$

The CFL condition (51) comes from the definition of the discrete energy:

$$E_h^{n+\frac{1}{2}} := \frac{1}{2}\left(\left\|D_{\Delta t} u_h^{n+\frac{1}{2}}\right\|^2_{\mathcal{T}^m} - \frac{\Delta t^2}{4}\left\|\partial_s D_{\Delta t} u_h^{n+\frac{1}{2}}\right\|^2_{\mathcal{T}^m}\right) + \frac{1}{2}\left\|\partial_s u_h^{n+\frac{1}{2}}\right\|^2_{\mathcal{T}^m},$$

which is positive when (51) holds. More precisely :

$$E_h^{n+\frac{1}{2}} \geq \frac{1}{2}\left(1 - C_{cfl}^2\right)\left\|D_{\Delta t} u_h^{n+\frac{1}{2}}\right\|^2_{\mathcal{T}^m} + \frac{1}{2}\left\|\partial_s u_h^{n+\frac{1}{2}}\right\|^2_{\mathcal{T}^m}. \tag{52}$$

Theorem 3.4 *Let (51) hold true and $f^n \in \mathrm{L}^2_\mu(\mathcal{T}^m)$, $n \in \mathbb{N}$. The scheme (48, 49) has a unique solution u_h^n, $n \in \mathbb{N}$. Moreover,*

$$\sqrt{E_h^{n+\frac{1}{2}}} \leq C\,\Delta t \sum_{k=1}^{n} \|f^k\|_{\mathcal{T}^m}, \tag{53}$$

where C depends on C_{cfl} only.

Proof It suffices to show the stability bound (53), which implies uniqueness. Then, the existence is obvious, since the problem is finite-dimensional.

The main trick for deriving the energy identity consists in writing

$$\left(\partial_s u_h^n, \partial_s v_h\right)_{\mathcal{T}^m} = \left(\left\{\partial_s u_h^n\right\}_{1/4}, \partial_s v_h\right)_{\mathcal{T}^m} - \frac{\Delta t^2}{4}\left(D_{\Delta t}^2\left(\partial_s u_h^n\right), \partial_s v_h\right)_{\mathcal{T}^m}. \tag{54}$$

Then, testing (48) written for $n = k$ with $v_h = D_{\Delta t} u_h^k$, yields

$$\frac{1}{\Delta t}\left(E_h^{k+\frac{1}{2}} - E_h^{k-\frac{1}{2}}\right) + \left\langle \left\{\mathcal{B}_m\left(\partial_t^{\Delta t}\right)\boldsymbol{\gamma}_m u_h^k\right\}_{1/4},\ D_{\Delta t}\boldsymbol{\gamma}_m u_h^k\right\rangle = \left(f^k,\ D_{\Delta t} u_h^k\right)_{\mathcal{T}^m}.$$

Summing the above in $k = 1, \ldots, n$, and using $E_h^{\frac{1}{2}} = 0$ results in

$$E_h^{n+\frac{1}{2}} + \Delta t \sum_{k=1}^{n} \left\langle \left\{\mathcal{B}_m\left(\partial_t^{\Delta t}\right)\boldsymbol{\gamma}_m u_h^k\right\}_{1/4},\ D_{\Delta t}\boldsymbol{\gamma}_m u_h^k\right\rangle = \Delta t \sum_{k=1}^{n}\left(f^k,\ D_{\Delta t} u_h^k\right)_{\mathcal{T}^m}. \tag{55}$$

Let us bound the right-hand side of the above via $E_h^{k+\frac{1}{2}}$, $k \le n$. First of all,

$$\begin{aligned}\left\| D_{\Delta t} u_h^k \right\|_{\mathcal{T}^m} &\le \frac{1}{2}\left(\left\| D_{\Delta t} u_h^{k+\frac{1}{2}} \right\|_{\mathcal{T}^m} + \left\| D_{\Delta t} u_h^{k-\frac{1}{2}} \right\|_{\mathcal{T}^m}\right)\\ &\overset{(52)}{\le} C\left(\sqrt{E_h^{k+\frac{1}{2}}} + \sqrt{E_h^{k-\frac{1}{2}}}\right).\end{aligned}$$

The above yields (where we again use $E_h^{\frac{1}{2}} = 0$)

$$\begin{aligned}\left|\Delta t \sum_{k=1}^{n}\left(f^k,\ D_{\Delta t} u_h^k\right)_{\mathcal{T}^m}\right| &\le C\Delta t\ \|f^n\|_{\mathcal{T}^m}\sqrt{E_h^{n+\frac{1}{2}}}\\ &\quad + C\Delta t \sum_{k=1}^{n-1}\left(\left\|f^k\right\|_{\mathcal{T}^m} + \left\|f^{k+1}\right\|_{\mathcal{T}^m}\right)\sqrt{E_h^{k+\frac{1}{2}}}.\end{aligned} \tag{56}$$

Since the last term in the left-hand side of (55) is non-negative (see (30) and Theorem 3.1), we deduce that

$$E_h^{n+\frac{1}{2}} \le C\Delta t\left(\|f^n\|_{\mathcal{T}^m}\sqrt{E_h^{n+\frac{1}{2}}} + \sum_{k=0}^{n-1}\left(\left\|f^k\right\|_{\mathcal{T}^m} + \left\|f^{k+1}\right\|_{\mathcal{T}^m}\right)\sqrt{E_h^{k+\frac{1}{2}}}\right).$$

A discrete Gronwall inequality (cf. [30, Appendix E]) yields the desired stability bound. □

Remark 3.4 Using the fact that the function μ is constant along each edge, it is straightforward to check that, if h denotes the smallest step of the mesh of $\mathcal{T}^m$, then, for some constant c_0 independent of μ, we have

$$C_{cfl}^2 \le c_0^2\,\frac{\Delta t^2}{h^2},$$

so that $c_0\Delta t/h < 1$ is a sufficient stability condition. Moreover, a finer analysis would also provide stability in the equality case, cf. e.g. [27, Chapter 6].

3.3.3 Error estimates for the time discretization

We compare in this section $u_h(t)$ and u_h^n. To simplify the computations we will assume that f satisfies (41).

Theorem 3.5 *Assume that f satisfies (41) and the CFL condition (51) holds. Let u_h and u_h^n be the solutions of (35) and (48, 49), respectively. Then, with $C(t^n) = c\max(1, t^n)^2$, where $c > 0$ depends only on C_{cfl},*

$$\left\|u_h(t^n) - u_h^n\right\|_{\mathcal{T}^m} \leq C(t^n)\,\Delta t^2 \int_0^{t^n} \left\|\partial_t^3 f\right\|_{\mathcal{T}^m} dt, \tag{57}$$

$$\left\|\partial_s u_h\left(t^{n+\frac{1}{2}}\right) - \partial_s u_h^{n+\frac{1}{2}}\right\|_{\mathcal{T}^m} \leq C(t^n)\,\Delta t^2 \int_0^{t^{n+1}} \left\|\partial_t^3 f\right\|_{\mathcal{T}^m} dt. \tag{58}$$

To prove the convergence of the time discretization, we will use the equivalence between (47) and (48), more precisely that u_h^n is the restriction to $\mathcal{T}^m$ of the solution $\bar{u}_h^n$ of (47). The existence of $\bar{u}_h^n$ the subject of the next lemma.

Lemma 3.5 [Well-posedness of (47)] *If f satisfies (41), there exists a unique sequence $\bar{u}_h^n \in X^h$, that solves (47) and satisfies $\bar{u}_h^0 = \bar{u}_h^1 = 0$.*

Proof The proof is slightly non-classical, because X^h is infinite-dimensional. On X^h we can define an equivalent scalar product:

$$(v, w)_{X^h} = \int_{\mathcal{T}} \mu(s) v(s) w(s) + \int_{\mathcal{T}\setminus\mathcal{T}^m} \mu(s)\,\partial_s v(s)\,\partial_s w(s). \tag{59}$$

Equipped with the above scalar product, X^h is a Hilbert space, because $X^h\big|_{\mathcal{T}^m} = U_h$, where U_h is a finite-dimensional space, and thus the respective norm is equivalent to the H^1_μ-norm on X^h. Let us next rewrite (47), by singling out terms with $\bar{u}_h^{n+1}$, cf. (59):

$$\begin{aligned}
&\left(\bar{u}_h^{n+1}, v_h\right)_{\mathcal{T}} + \frac{\Delta t^2}{4}\left(\partial_s \bar{u}_h^{n+1}, \partial_s v_h\right)_{\mathcal{T}\setminus\mathcal{T}^m} = \left\langle \ell_h^n, v_h\right\rangle \quad \forall\, v_h \in X^h,\\
&\text{where } \left\{\begin{aligned}
\langle \ell_h^n, v_h\rangle &:= \Delta t^2\,(f^n, v_h)_{\mathcal{T}^m}\\
&\quad + \left(2\bar{u}_h^n - \bar{u}_h^{n-1}, v_h\right)_{\mathcal{T}} - \Delta t^2\left(\partial_s \bar{u}_h^n, \partial_s v_h\right)_{\mathcal{T}^m}\\
&\quad - \left(\Delta t^2/4\right)\left(\partial_s(2\,\bar{u}_h^n + \bar{u}_h^{n-1}), \partial_s v_h\right)_{\mathcal{T}\setminus\mathcal{T}^m}.
\end{aligned}\right.
\end{aligned} \tag{60}$$

Note that $\langle \ell_h^n, v_h\rangle$ defines a bounded linear functional on X^h; in particular,

$$\left|\left(\partial_s \bar{u}_h^n, \partial_s v_h\right)_{\mathcal{T}^m}\right| \leq C(h)\,\|\bar{u}_h\|_{\mathcal{T}^m}\|v_h\|_{\mathcal{T}^m},$$

because $\bar{u}_h|_{\mathcal{T}^m}$, $v_h|_{\mathcal{T}^m} \in U_h$. The existence and uniqueness of the solution to the above thus follows from Lax–Milgram's lemma (cf. (59)). □

Based on the definition of the discrete transparent boundary conditions, cf. Sect. 3.1.1, and the proof of Lemma 3.2 in the semi-discrete case, we can state the following result.

Lemma 3.6 *The solution* $(\bar{u}_h^n)_{n\in\mathbb{N}}$ *of* (47) *with the initial conditions* $\bar{u}_h^0 = \bar{u}_h^1 = 0$ *and the solution* $(u_h^n)_{n\in\mathbb{N}}$ *of* (48, 49) *satisfy* $\bar{u}_h^n|_{\mathcal{T}^m} = u_h^n$, $n \in \mathbb{N}$.

The stability of (47) relies, like for (48), on an energy estimate. Let us define

$$\overline{E}_h^{n+\frac{1}{2}} := \frac{1}{2}\left(\left\|D_{\Delta t}\bar{u}_h^{n+\frac{1}{2}}\right\|_{\mathcal{T}}^2 - \frac{\Delta t^2}{4}\left\|\partial_s D_{\Delta t}\bar{u}_h^{n+\frac{1}{2}}\right\|_{\mathcal{T}^m}^2\right) + \frac{1}{2}\left\|\partial_s \bar{u}_h^{n+\frac{1}{2}}\right\|_{\mathcal{T}}^2,$$

which satisfies (as in (52))

$$\overline{E}_h^{n+\frac{1}{2}} \geq \frac{1-C_{cfl}^2}{2}\left\|D_{\Delta t}\bar{u}_h^{n+\frac{1}{2}}\right\|_{\mathcal{T}^m}^2 + \frac{1}{2}\left\|D_{\Delta t}\bar{u}_h^{n+\frac{1}{2}}\right\|_{\mathcal{T}\setminus\mathcal{T}^m}^2 + \frac{1}{2}\left\|\partial_s \bar{u}_h^{n+\frac{1}{2}}\right\|_{\mathcal{T}}^2. \tag{61}$$

Then, proceeding as in Theorem 3.4, one easily proves

Lemma 3.7 [Stability of (47)] *Under the assumptions of Theorem 3.5, one has, with* $C > 0$ *depending on* C_{cfl} *only, for all* $n \in \mathbb{N}$,

$$\sqrt{\overline{E}_h^{n+\frac{1}{2}}} \leq C\Delta t \sum_{k=1}^{n} \|f^k\|. \tag{62}$$

We now have all the auxiliary results needed to prove Theorem 3.5.

Proof of Theorem 3.5 By Lemmas 3.2 and 3.6, instead of comparing u_h^n with $u_h(t^n)$, we will compare the solution $\bar{u}_h^n$ of (47) with initial conditions $\bar{u}_h^0 = \bar{u}_h^1 = 0$ with $\bar{u}_h(t^n)$ solving (37). The proof is not fully standard, because in one part of the domain an explicit scheme is used, while an implicit scheme is employed in the other part.

Step 1: Error bound in the energy norm. The error $\bar{e}_h^n = \bar{u}_h^n - \bar{u}_h(t^n) \in X^h$ satisfies, for any $v_h \in X^h$,

$$\begin{aligned}&\left(D_{\Delta t}^2 \bar{e}_h^n, v_h\right)_{\mathcal{T}} + \left(\partial_s \bar{e}_h^n, \partial_s v_h\right)_{\mathcal{T}^m} + \left(\partial_s\left\{\bar{e}_h^n\right\}_{1/4}, \partial_s v_h\right)_{\mathcal{T}\setminus\mathcal{T}^m}\\ &\quad = -\left(D_{\Delta t}^2 \bar{u}_h(t^n) - \partial_t^2 \bar{u}_h(t^n), v_h\right)_{\mathcal{T}} - \left(\partial_s\left(\{\bar{u}_h(t^n)\}_{1/4} - \bar{u}_h(t^n)\right), \partial_s v_h\right)_{\mathcal{T}\setminus\mathcal{T}^m},\end{aligned} \tag{63}$$

with the initial condition $\bar{e}_h^0 = 0$, and $\bar{e}_h^1 = \bar{u}_h^1 - \bar{u}_h(t^1) \equiv -\bar{u}_h(t^1)$ to be quantified later. Let us introduce the *truncation errors*

$$\delta_h^n := D_{\Delta t}^2 \bar{u}_h(t^n) - \partial_t^2 \bar{u}_h(t^n), \quad \varepsilon_h^n := \partial_s\left(\{\bar{u}_h(t^n)\}_{1/4} - \bar{u}_h(t^n)\right).$$

Testing (63), written for $n = k$, with $v_h = D_{\Delta t}\bar{e}_h^k$, we obtain (with (54) again)

$$\frac{\overline{E}_e^{k+\frac{1}{2}} - \overline{E}_e^{k-\frac{1}{2}}}{\Delta t} = -\left(\delta_h^k, D_{\Delta t}\bar{e}_h^k\right)_{\mathcal{T}} - \left(\varepsilon_h^k, D_{\Delta t}\partial_s\bar{e}_h^k\right)_{\mathcal{T}\setminus\mathcal{T}^m}, \tag{64}$$

where $\overline{E}_e^{k+\frac{1}{2}}$ is the discrete energy of the error $\bar{e}_h^k$:

$$\overline{E}_e^{n+\frac{1}{2}} := \frac{1}{2}\left(\left\|D_{\Delta t}\bar{e}_h^{n+\frac{1}{2}}\right\|_{\mathcal{T}}^2 - \frac{\Delta t^2}{4}\left\|\partial_s D_{\Delta t}\bar{e}_h^{n+\frac{1}{2}}\right\|_{\mathcal{T}^m}^2\right) + \frac{1}{2}\left\|\partial_s\bar{e}_h^{n+\frac{1}{2}}\right\|_{\mathcal{T}}^2.$$

Summing (64) in $k = 1, \ldots, n$, and next applying a discrete integration by parts to the sum involving $D_{\Delta t}\partial_s e_h^k$, we end up with the following identity:

$$\begin{aligned}\overline{E}_e^{n+\frac{1}{2}} = \overline{E}_e^{\frac{1}{2}} - \Delta t\sum_{k=1}^{n}\left(\delta_h^k, D_{\Delta t}\bar{e}_h^k\right)_{\mathcal{T}} - \left(\varepsilon_h^n, \partial_s\bar{e}_h^{n+\frac{1}{2}}\right)_{\mathcal{T}\setminus\mathcal{T}^m} + \left(\varepsilon_h^1, \partial_s\bar{e}_h^{1/2}\right)_{\mathcal{T}\setminus\mathcal{T}^m}\\ + \Delta t\sum_{k=1}^{n-1}\left(\frac{\varepsilon_h^{k+1}-\varepsilon_h^k}{\Delta t}, \partial_s\bar{e}_h^{k+\frac{1}{2}}\right)_{\mathcal{T}\setminus\mathcal{T}^m}.\end{aligned}$$

The right hand side can be bounded using (61) and the Cauchy–Schwarz inequality (see also the proof of Theorem 3.4):

$$\begin{aligned}\overline{E}_e^{n+\frac{1}{2}} \le\ & \overline{E}_e^{\frac{1}{2}} + \Delta t\left\|\delta_h^n\right\|\sqrt{\overline{E}_e^{n+\frac{1}{2}}}\\ & + C\left(\Delta t\sum_{k=0}^{n-1}\frac{\left\|\delta_h^k\right\| + \left\|\delta_h^{k+1}\right\|}{2}\sqrt{\overline{E}_e^{k+\frac{1}{2}}} + \left\|\varepsilon_h^n\right\|_{\mathcal{T}\setminus\mathcal{T}^m}\sqrt{\overline{E}_e^{n+\frac{1}{2}}}\right.\\ & \left. + \left\|\varepsilon_h^1\right\|_{\mathcal{T}\setminus\mathcal{T}^m}\sqrt{\overline{E}_e^{\frac{1}{2}}} + \Delta t\sum_{k=1}^{n-1}\left\|\frac{\varepsilon_h^{k+1}-\varepsilon_h^k}{\Delta t}\right\|_{\mathcal{T}\setminus\mathcal{T}^m}\sqrt{\overline{E}_e^{k+\frac{1}{2}}}\right).\end{aligned}$$

The constant C depends on the CFL (51). Applying to the above a discrete Gronwall inequality (see [30, Appendix E]), we obtain (with a different constant $C > 0$):

$$\begin{aligned}\sqrt{\overline{E}_e^{n+\frac{1}{2}}} \le \sqrt{\overline{E}_e^{\frac{1}{2}}} + C\max_{1\le k\le n}\left\|\varepsilon_h^k\right\|_{\mathcal{T}\setminus\mathcal{T}^m} + C\,\Delta t\sum_{k=1}^{n}\left\|\delta_h^k\right\|\\ + C\,\Delta t\sum_{k=1}^{n-1}\left\|\frac{\varepsilon_h^{k+1}-\varepsilon_h^k}{\Delta t}\right\|_{\mathcal{T}\setminus\mathcal{T}^m}.\end{aligned} \tag{65}$$

Step 2: Bounding the error stemming from initial conditions. This is classical. One simply uses Taylor expansions and a priori estimates of $\bar{u}_h(t)$, as a solution of (37),

similar to the ones of Corollary 2.1, to get

$$\sqrt{\overline{E}_e^{\frac{1}{2}}} \leq C\,\Delta t^2 \int_0^{\Delta t} \left\| \partial_\tau^3 f(\tau) \right\|_{\mathcal{T}^m} d\tau. \tag{66}$$

Step 3: Bounding in (65) *the terms due to the consistency errors.* To obtain a bound on the right-hand side of (65), we use the Taylor theorem again:

$$\begin{aligned} \left\| \delta_h^k \right\| &\leq c\,\Delta t^2 \sup_{t\in(t^{k-1},t^{k+1})} \left\| \partial_t^4 \bar{u}_h(t) \right\|, \\ \left\| \varepsilon_h^k \right\|_{\mathcal{T}\setminus\mathcal{T}^m} &\leq c\,\Delta t^2 \sup_{t\in(t^{k-1},t^{k+1})} \left\| \partial_t^2 \partial_s \bar{u}_h(t) \right\|_{\mathcal{T}\setminus\mathcal{T}^m}, \\ \left\| \frac{\varepsilon_h^k - \varepsilon_h^{k-1}}{\Delta t} \right\|_{\mathcal{T}\setminus\mathcal{T}^m} &\leq c\,\Delta t^2 \sup_{t\in(t^{k-1},t^{k+1})} \left\| \partial_t^3 \partial_s \bar{u}_h(t) \right\|_{\mathcal{T}\setminus\mathcal{T}^m}. \end{aligned} \tag{67}$$

Step 4: Bounding the energy of the error. Substituting (66) and (67) into (65) results in (for some $C > 0$),

$$\begin{aligned} \sqrt{\overline{E}_e^{n+\frac{1}{2}}} \leq\; & C\,\Delta t^2 \int_0^{\Delta t} \left\| \partial_t^3 f \right\|_{\mathcal{T}^m} dt + C\,\Delta t^2 \sup_{t\in(0,t^{n+1})} \left\| \partial_t^2 \partial_s \bar{u}_h(t) \right\|_{\mathcal{T}\setminus\mathcal{T}^m} \\ & + C\,t^n \Delta t^2 \left(\sup_{t\in(0,t^{n+1})} \left\| \partial_t^3 \partial_s \bar{u}_h(t) \right\|_{\mathcal{T}\setminus\mathcal{T}^m} + \sup_{t\in(0,t^{n+1})} \left\| \partial_t^4 \bar{u}_h(t) \right\|_{\mathcal{T}\setminus\mathcal{T}^m} \right). \end{aligned}$$

Applying again a priori estimates for $\bar{u}_h$ similar to the ones of Corollary 2.1, we obtain the following bound, with $C > 0$ depending on C_{cfl}:

$$\sqrt{\overline{E}_e^{n+\frac{1}{2}}} \leq C\,\Delta t^2 \max(1, t^{n+1}) \left\| \partial_t^3 f \right\|_{L^1\left(0,t^{n+1};\mathrm{L}^2_\mu(\mathcal{T}^m)\right)}. \tag{68}$$

Step 5: Derivation of (57, 58). Combining (68) with (61) yields, with $\widetilde{C} > 0$ depending on C_{cfl},

$$\left\| \frac{\bar{e}_h^{n+1} - \bar{e}_h^n}{\Delta t} \right\|_{\mathcal{T}} + \left\| \partial_s \bar{e}_h^{n+\frac{1}{2}} \right\|_{\mathcal{T}} \leq \widetilde{C}\,\Delta t^2 \max(1, t^{n+1}) \| f \|_{L^1\left(0,t^{n+1};\mathrm{L}^2_\mu(\mathcal{T})\right)}. \tag{69}$$

A classical argument of telescopic sums (with $C(t^n)$ as in the statement of the theorem) yields

$$\left\| \bar{e}_h^n \right\|_{\mathcal{T}^m} = \left\| \bar{u}_h(t^n) - \bar{u}_h^n \right\|_{\mathcal{T}^m} \leq C(t^n)\,\Delta t^2 \int_0^{t^n} \left\| \partial_t^3 f \right\|_{\mathcal{T}^m} dt. \tag{70}$$

Next, writing

$$\bar{u}_h\left(t^{n+\frac{1}{2}}\right) - \bar{u}_h^{n+\frac{1}{2}} = \bar{e}_h^{n+\frac{1}{2}} + \left(\bar{u}_h\left(t^{n+\frac{1}{2}}\right) - \frac{\bar{u}_h(t^{n+1}) + \bar{u}_h(t^n)}{2}\right),$$

and then using (69) and Taylor estimates, we obtain (the details are omitted)

$$\left\|\partial_s\left(u_h\left(t^{n+\frac{1}{2}}\right) - u_h^{n+\frac{1}{2}}\right)\right\|_{\mathcal{T}} \le C(t^n)\,\Delta t^2 \int_0^{t^{n+1}} \left\|\partial_t^3 f\right\|_{\mathcal{T}^m} dt. \tag{71}$$

To obtain the bounds (57, 58) we use (70, 71) and the fact $u_h(t)$ and u_h^n are the restrictions of respectively $\bar{u}_h(t)$ and $\bar{u}_h^n$ to $\mathcal{T}^m$ (Lemmas 3.2, 3.6). □

Remark 3.5 We used a direct time domain approach. An alternative approach is to use convergence estimates for the trapezoid rule discretization of the operator $\mathcal{B}_m(\partial_t)$, see [3, Appendix A] or a recent work [19,20], based on frequency dependent coercivity/continuity bounds on the symbol $\mathcal{B}_m(\omega)$. However often this approach leads to non-optimal estimates in terms of the powers of the final time T

3.3.4 Convergence of the time and space discretizations

From Theorems 3.3 and 3.5 and the triangle inequality, we deduce

Theorem 3.6 *Assume that f satisfies (41) and the CFL condition (51) holds. Let u_m be a solution of (17) and u_h^n the solution of (48, 49). Then, with $C(t^n) = c\max(1, t^n)^2$, where $c > 0$ depends on the CFL only, the following error bound holds:*

$$\left\|u_m(t^n) - u_h^n\right\|_{\mathcal{T}^m} \le C(t^n)\left(\Delta t^2 + h\right)\|f\|_{W^{3,1}\left(0,t^n;\mathrm{L}^2_\mu(\mathcal{T}^m)\right)}, \tag{72}$$

$$\left\|\partial_s\left(u_m\left(t^{n+\frac{1}{2}}\right) - u_h^{n+\frac{1}{2}}\right)\right\|_{\mathcal{T}^m} \le C(t^n)(\Delta t^2 + h)\|f\|_{W^{3,1}\left(0,\,t^{n+1};\mathrm{L}^2_\mu(\mathcal{T}^m)\right)}. \tag{73}$$

3.4 Solving the fully discrete system (48, 49). Complexity

In practice, to solve (48), we use the mass lumped FEM. This renders the respective system fully explicit. In fact, the only implicit terms are the boundary ones, which are essentially one-dimensional (and in total there are $p^m = O(1)$ of such terms). To see this, let us assume that $\ell > 0$ is s.t. (with an abuse of notation: ℓ here is a spatial index, rather than m from $\mathcal{T}^m$) u_ℓ^n is a nodal value of u_h^n in $M_{m,j}$, and $u_{\ell-1}^n$ is the nodal value in the closest to $M_{m,j}$ node. Then the mass-lumped (48) for u_ℓ^{n+1} reads

$$\frac{u_\ell^{n+1} - 2u_\ell^n + u_\ell^{n-1}}{(\Delta t)^2} + 2\frac{u_\ell^n - u_{\ell-1}^n}{h^2}$$

$$+\frac{1}{2h}\left(\sum_{k=0}^{n+1} b^{\Delta t}_{m,j;k} u^{n+1-k}_{\ell} + 2\sum_{k=0}^{n} b^{\Delta t}_{m,j;k} u^{n-k}_{\ell} + \sum_{k=0}^{n-1} b^{\Delta t}_{m,j;k} u^{n-1-k}_{\ell}\right) = 0,$$

see (32) for the definition of the convolution weights $b^{\Delta t}_{m,j;k}$. It is easy to see that the above can be written in an explicit form. This nonetheless requires evaluating several discrete convolutions, each of $O(n)$ size, in order to compute the right-hand side. Provided that the spatial discretization has N_s degrees of freedom, the total complexity of computing the solution to (48, 49) for N_t time steps is thus $O(N_t N_s) + O(N_t^2)$, where $O(N_t^2)$ comes from the computation of the convolutions in the boundary terms.

4 Convolution quadrature: computing convolution weights

One of the major practical difficulties of the application of the CQ is linked to the computation of convolution weights $\boldsymbol{b}^{\Delta t}_{m,n}$, that is to say, $\lambda^{\Delta t}_n$, cf. (32), particularly in our case, since the symbol $\boldsymbol{\Lambda}(\omega)$ is not known explicitly.

4.1 Classical FFT-based algorithm for computing convolution weights

The convolution weights for $\mathcal{B}_m(\partial_t)$ can be expressed via the reference DtN convolution weights, see (32). The latter, in turn, can be evaluated by discretizing the Cauchy integral (28), first by choosing the contour γ as a circle of radius ρ, and next using a quadrature. To compute $N_t + 1$ weights, we apply the trapezoid quadrature with N quadrature points (where $N \geq N_t + 1$):

$$\lambda^{\Delta t}_n \approx \frac{\rho^{-n}}{N}\sum_{k=0}^{N-1} \mathrm{e}^{-i\frac{2\pi kn}{N}} \boldsymbol{\Lambda}(\omega_k), \quad \omega_k = i\frac{\delta\left(\rho \mathrm{e}^{i\frac{2\pi k}{N}}\right)}{\Delta t}, \quad n = 0, \ldots, N_t. \tag{74}$$

While the value of (28) does not depend on ρ, this is not the case for the above approximation. An optimal choice of ρ is ensured by minimizing the numerical error in the above expression, which is the sum of the quadrature error $O(\rho^N)$ and the error stemming from the numerical computation of the value $\boldsymbol{\Lambda}(\omega)$, estimated by $O(\rho^{-N_t}\varepsilon)$, cf. (74), where ε is the accuracy of evaluation of $\boldsymbol{\Lambda}(\omega)$. Crucially, this latter error can not be smaller than the machine epsilon. More details can be found in [3,7,38]; see as well Sect. 4.3.1. In particular, the choice $N = N_t + 1$ and $\rho = \varepsilon^{\frac{1}{2N}}$ results in the error $O(\sqrt{\varepsilon})$.

Obviously, (74) can be easily computed via the FFT. Provided that the computational cost of evaluation of $\boldsymbol{\Lambda}(\omega_k)$ for all $k = 0, \ldots, N_t$ is bounded by $c_{\boldsymbol{\Lambda}}$, the above computations require $O(N_t \log N_t)$ time to perform the FFT, and $O(N_t c_{\boldsymbol{\Lambda}})$ complexity to evaluate all $\boldsymbol{\Lambda}(\omega_k)$. Of course, these costs depend on the frequencies ω_k, and, just like in the case of the exterior problem for the wave equation, cf. [3,4], increase with $\Delta t \to 0$. One of the main goals of this section is to quantify the efficiency of the CQ method for the approximation of the transparent BCs in fractal trees. This section is organized as follows:

– in Sect. 4.2 we present an algorithm to evaluate $\mathbf{\Lambda}(\omega)$, and very briefly discuss its stability, convergence and complexity. In the end, we will demonstrate how $\mathbf{\Lambda}(\omega)$ can be approximated efficiently when $\mathrm{Im}\,\omega$ is large enough.

– in Sect. 4.3 we will discuss the numerical aspects of (74), in particular, the dependence of the evaluation error of $\lambda_n^{\Delta t}$ on the evaluation error of $\mathbf{\Lambda}(\omega)$, and, as a result, the choice of the parameters in (74). Next, we will present a strategy to compute convolution weights, and then provide the respective asymptotic complexity bounds, as $\Delta t \to 0$.

Remark 4.1 When $\Delta t \to 0$, $|\mathbf{\Lambda}(\omega_k)| \sim |\omega_k|$, cf. Theorem 2.4. Since the frequencies $|\omega_k|$ grow at least as $O((\Delta t)^{-1})$ (cf. (74)), to preserve the $O(1)$ scaling as $\Delta t \to 0$, instead of computing the convolution weights for $\mathbf{\Lambda}(\omega)$, we compute the convolution weights for the scaled quantity $\mathbf{\Lambda}^s(\omega) := (-i\omega)^{-1}\mathbf{\Lambda}(\omega)$ (hence the use of the index 's' for 'scaled'). This can be incorporated into the coupled formulation (48, 49) as follows.

With (30), see also (29) and the explanation below for the notation, denoting by $\partial_t^{\Delta t}\Lambda^s\left(\alpha_{m,j}\alpha_k\partial_t^{\Delta t}\right)$ a discrete convolution operator with the discrete symbol $\frac{\delta(z)}{\Delta t}\mathbf{\Lambda}^s\left(i\alpha_{m,j}\alpha_k\frac{\delta(z)}{\Delta t}\right)$, we have

$$\mathcal{B}_{m,j}\left(\partial_t^{\Delta t}\right) = \mu_{m,j}\,\alpha_{m,j}^{-1}\sum_{k=0}^{p-1}\frac{\mu_k}{\alpha_k}\alpha_{m,j}\alpha_k\partial_t^{\Delta t}\Lambda^s\left(\alpha_{m,j}\alpha_k\partial_t^{\Delta t}\right),$$

Let $\mathcal{B}^s_{m,j}(\partial_t^{\Delta t}) := \mu_{m,j}\sum_{k=0}^{p-1}\mu_k\Lambda^s\left(\alpha_{m,j}\alpha_k\partial_t^{\Delta t}\right)$, so that

$$\mathcal{B}_{m,j}\left(\partial_t^{\Delta t}\right) \equiv \partial_t^{\Delta t}\mathcal{B}^s_{m,j}\left(\partial_t^{\Delta t}\right). \tag{75}$$

The corresponding aggregate operator $\mathcal{B}^s_m(\partial_t^{\Delta t})$ is defined like in (11); see also Sect. 3.1.2. In the final discretization (48, 49), it suffices to replace

$$\left\{\mathcal{B}_m\left(\partial_t^{\Delta t}\right)\boldsymbol{\gamma}_m u^n\right\}_{\frac{1}{4}} \text{ by } D_{\Delta t}\left(\mathcal{B}^s_m\left(\partial_t^{\Delta t}\right)\boldsymbol{\gamma}_m u^n\right). \tag{76}$$

To see this, by the injectivity property of the Z-transform, it suffices to verify that for any sequence $(v^n)_{n\in\mathbb{N}}$, the Z-transform of $D_{\Delta t}\left(\mathcal{B}^s_m(\partial_t^{\Delta t})\boldsymbol{\gamma}_m v^n\right)$ coincides with the Z-transform of $\{\mathcal{B}_m(\partial_t^{\Delta t})\boldsymbol{\gamma}_m v^n\}_{\frac{1}{4}}$. This is indeed the case: for all $j = 0, \ldots, p^m - 1$, we have

$$\begin{aligned} Z\left\{\mathcal{B}_{m,j}\left(\partial_t^{\Delta t}\right)v^n\right\}_{\frac{1}{4}} &= \frac{z^{-1}+2+z}{4}\boldsymbol{\mathcal{B}}_{m,j}\left(i\frac{\delta(z)}{\Delta t}\right)V(z) \\ &\overset{(75)}{=} \frac{z^{-1}+2+z}{4}\left(\frac{\delta(z)}{\Delta t}\right)\boldsymbol{\mathcal{B}}^s_{m,j}\left(i\frac{\delta(z)}{\Delta t}\right)V(z) \end{aligned}$$

$$= \frac{z^{-1} - z}{2\Delta t} \mathcal{B}^s_{m,j} \left(i \frac{\delta(z)}{\Delta t} \right) V(z),$$

where to obtain the last expression we used the explicit form of $\delta(z) = 2\frac{1-z}{1+z}$. We finally remark that the last expression in the above is nothing more than $Z\left(D_{\Delta t}\mathcal{B}^s_{m,j}(\partial_t^{\Delta t})v^n\right)$.

4.2 Evaluation of $\mathbf{\Lambda}(\omega)$

4.2.1 A method for computing $\mathbf{\Lambda}(\omega)$

The method for computing $\mathbf{\Lambda}$ presented in this section resembles the method of [33], which aims at approximating $\mathbf{\Lambda}$ in a domain of $\mathbb{C}^+ = \{\omega : \operatorname{Im}\omega > 0\}$. However, the approach of this article is better suited to the case when a highly accurate evaluation of $\mathbf{\Lambda}$ at a set of points on a curve in a complex plane is needed, like in (74). It is based on the following ideas:

- to be able to evaluate $\mathbf{\Lambda}(\omega)$, it suffices to know the values of $\mathbf{\Lambda}(\alpha_i\omega), i = 0, \ldots, p-1$ (i.e., for p 'smaller' frequencies), cf. Lemma 2.1;
- for $|\omega| < r$, where r is a fixed value smaller than the first pole of $\mathbf{\Lambda}$, $\mathbf{\Lambda}(\omega)$ can be accurately approximated by $2N_* + 2$ first terms of its Taylor expansion in zero. Provided even coefficients $\{\lambda_{2n}\}_{n\in\mathbb{N}}$ of the Taylor series for $\mathbf{\Lambda}$ in $\omega = 0$ ($\mathbf{\Lambda}$ is even by Theorem 2.4), this approximation reads

$$\mathbf{\Lambda}(\omega) \approx \sum_{n=0}^{N_*} \lambda_{2n}\, \omega^{2n}. \tag{77}$$

  The coefficients λ_{2n} can be computed recursively, cf. [33, Appendix C].

To formulate the algorithm, let us fix $\omega \in \mathbb{C}^+$ for which we need to evaluate $\mathbf{\Lambda}(\omega)$, and introduce the following sets:

$$\mathcal{L}_n(\omega) := \left\{ \mathbf{\Lambda}\left(\alpha_0^{k_0} \ldots \alpha_{p-1}^{k_{p-1}}\omega\right) : 0 \le k_i \le n,\ i = 0, \ldots, p-1,\ \sum_{i=0}^{p-1} k_i = n \right\}.$$

These sets possess the following properties:

(a) the set $\mathcal{L}_0(\omega) = \{\mathbf{\Lambda}(\omega)\}$.
(b) provided that the values in $\mathcal{L}_n(\omega)$ are known, it is possible to compute all the elements in $\mathcal{L}_{n-1}(\omega)$ using the expression (15) (rewritten below, cf. (78)) and the elements of $\mathcal{L}_n(\omega)$.

$$\mathbf{\Lambda}(\omega) = -\omega \frac{\omega \tan\omega - \mathbf{F}_{\alpha,\mu}(\omega)}{\tan\omega \mathbf{F}_{\alpha,\mu}(\omega) + \omega}, \quad \mathbf{F}_{\alpha,\mu}(\omega) = \sum_{i=0}^{p-1} \frac{\mu_i}{\alpha_i} \mathbf{\Lambda}(\alpha_i\omega). \tag{78}$$

This is immediate when $n = 1$, and not difficult to check for $n > 1$.

(c) in $\mathcal{L}_n(\omega)$, there are $C_{n+p-1}^{p-1} = O(n^p)$ elements.

Given r as described before (77), let us assume that $|\omega| > r$ and fix $L \in \mathbb{N}$ s.t.

$$|\boldsymbol{\alpha}|_\infty^L \, |\omega| < r, \quad \text{i.e. } L := L(\omega, r) = \left\lfloor \left(\log |\boldsymbol{\alpha}|_\infty^{-1} \right)^{-1} \log \frac{|\omega|}{r} \right\rfloor + 1. \tag{79}$$

The above ensures that all the arguments of $\boldsymbol{\Lambda}(.)$ in $\mathcal{L}_L(\omega)$ satisfy:

$$\prod_{\ell=0}^{p-1} \alpha_\ell^{k_\ell} \, |\omega| \le (|\boldsymbol{\alpha}|_\infty)^{\sum_{\ell=0}^{p-1} k_\ell} \, |\omega| = |\boldsymbol{\alpha}|_\infty^L |\omega| < r.$$

Knowing all the elements in the set $\mathcal{L}_L(\omega)$, we can compute exactly the elements of $\mathcal{L}_{L-1}(\omega)$, then $\mathcal{L}_{L-2}(\omega)$, and so on, up to $\boldsymbol{\Lambda}(\omega)$. The method presented here is based on this idea, with the only modification that the elements in $\mathcal{L}_L(\omega)$ are approximated with the help of (77). The respective approximation of the sets $\mathcal{L}_n(\omega)$ will be denoted by $\mathcal{L}_n^*(\omega) = \mathcal{L}_n^*$.

Given $\boldsymbol{k} = (k_0, \ldots, k_{p-1})$, by $\boldsymbol{\Lambda}_{\boldsymbol{k}} = \boldsymbol{\Lambda}_{k_0,\ldots,k_{p-1}}$ we will denote an approximation to $\boldsymbol{\Lambda}\left(\prod_{\ell=0}^{p-1} \alpha_\ell^{k_\ell} \omega\right)$.

procedure EVALLAMBDA(ω, N_*, r, $\{\lambda_{2n}\}_{n=0}^{N_*}$)
  for $n = L, \, L-1, \ldots, 0$ **do**
    if $n = L$ **then**
      $\mathcal{L}_L^* := \emptyset$
      for $k_i : 0 \le k_i \le L, \, i = 0, \ldots, p-1, \, \sum_{i=0}^{p-1} k_i = L$ **do**
        $\boldsymbol{k} := (k_0, \ldots, k_{p-1})$
        $\omega_{\boldsymbol{k}} := \prod_{i=0}^{p-1} \alpha_i^{k_i} \omega$
        $\boldsymbol{\Lambda}_{\boldsymbol{k}} := \sum_{n=0}^{N_*} \lambda_{2n} \omega_{\boldsymbol{k}}^{2n}$, see (77)
        $\mathcal{L}_L^* := \mathcal{L}_L^* \cup \{\boldsymbol{\Lambda}_{\boldsymbol{k}}\}$
    else
      $\mathcal{L}_n^* := \emptyset$
      for $k_i : 0 \le k_i \le n, \, i = 0, \ldots, p-1, \, \sum_{i=0}^{p-1} k_i = n$ **do**
        $\boldsymbol{k} := (k_0, \ldots, k_{p-1})$
        $\omega_{\boldsymbol{k}} := \prod_{i=0}^{p-1} \alpha_i^{k_i} \omega$
        $\mathbf{F}_{\boldsymbol{k}}^* := \sum_{\ell=0}^{p-1} \frac{\mu_\ell}{\alpha_\ell} \boldsymbol{\Lambda}_{k_0,k_1,\cdots,k_{\ell-1},k_\ell+1,k_{\ell+1},\cdots,k_{p-1}}$

▷ Remark: $\mathbf{\Lambda}_{k_0,k_1,\cdots,k_{\ell-1},k_\ell+1,k_{\ell+1},\cdots,k_{p-1}} \in \mathcal{L}^*_{n+1}$ for all $\ell = 0, \ldots, p-1$

▷ Remark: $\mathbf{F}^*_{\boldsymbol{k}}$ plays a role of $\boldsymbol{F}_{\alpha,\mu}(\omega_{\boldsymbol{k}})$ in (78)

16: $\quad \mathbf{\Lambda}_{\boldsymbol{k}} := -\omega_{\boldsymbol{k}} \dfrac{\omega_{\boldsymbol{k}} \tan \omega_{\boldsymbol{k}} - \mathbf{F}^*_{\boldsymbol{k}}}{\tan \omega_{\boldsymbol{k}} \mathbf{F}^*_{\boldsymbol{k}} + \omega_{\boldsymbol{k}}}$, see (78)

17: $\quad \mathcal{L}^*_n := \mathcal{L}^*_n \cup \{\mathbf{\Lambda}_{\boldsymbol{k}}\}$

return $\mathcal{L}^*_0$

Remark 4.2 A somewhat tricky part in the practical implementation of the above procedure is arranging and accessing the computed values in the sets $\mathcal{L}^*_n$; this nonetheless can be done efficiently (with extra memory costs) as described e.g. in [30].

Remark 4.3 In the above algorithm, the choice whether the DtN for the Dirichlet or Neumann problem is computed is encoded in the coefficients $\{\lambda_{2n}\}_{n=0}^{N_*}$.

4.2.2 Well-definiteness and convergence of the method of Sect. 4.2.1

Well-definiteness One could wonder whether using (78) may result in division by zero in the course of **EvalLambda**. The answer is given below.

Proposition 4.1 *There exists $r_0 > 0$, s.t. for all $r < r_0$, $N_* \geq 0$, for all $\omega \in \mathbb{C}^+$, no division by zero occurs in the course of the procedure **EvalLambda** $(\omega, N_*, r, \{\lambda_{2n}\}_{n=0}^{N_*})$.*

Proof See the report [30]. This statement generalizes Lemma 5.15 in [33] and is based on the preservation of the positivity property (cf. Theorem 2.4(a)) of the approximate DtN .

□

Error estimates There are two parameters in the method that affect its accuracy: N_* and r. Let us denote by $\mathbf{\Lambda}_{r,N_*}(\omega)$ the value computed with the help of the procedure **EvalLambda** $(\omega, N_*, r, \{\lambda_{2n}\}_{n=0}^{N_*})$, and let

$$E_{r,N_*}(\omega) := \left|\mathbf{\Lambda}_{r,N_*}(\omega) - \mathbf{\Lambda}(\omega)\right|.$$

To formulate the error estimates, let us introduce the following notations. First of all, let us fix a parameter $\rho > 0$ that can be chosen arbitrarily from

$$\rho \in (0, \omega_0), \tag{80}$$

where ω_0 is the smallest positive pole of $\mathbf{\Lambda}(\omega)$. Let also

$$N_0 = \min\left\{\ell \geq 0 : \sum_{i=0}^{p-1} \mu_i \alpha_i^{2\ell+1} < 1\right\}. \tag{81}$$

Then, provided $r > 0$, we denote the exterior of $\mathcal{B}_r(0)$ in $\mathbb{C}^+$ by

$$\mathbb{C}^+_r := \{z \in \mathbb{C}^+ : |z| > r\}.$$

Because we will be interested in approximating $\mathbf{\Lambda}(\omega)$ for ω s.t. $\operatorname{Im}\omega > a > 0$, with a being fixed, let us additionally define

$$\mathbb{C}^+_{a,r} := \left\{z \in \mathbb{C}^+_r : \operatorname{Im}\omega \geq a\right\}, \quad a \in (0, 1]. \tag{82}$$

Obviously, for any $r > 0$, any $\omega \in \mathbb{C}^+$, we have:

$$\text{either } \omega \in \mathbb{C}^+ \cap \overline{\mathcal{B}_r(0)} \quad \text{or} \quad \omega \in \mathbb{C}^+_{a,r}, \ \text{ where } a = \min(1, \operatorname{Im}\omega).$$

Next, we state the dependence of $E_{r,N_*}(\omega)$ on r, N_* separately in two cases: the case $\omega \in \mathbb{C}^+ \cap \overline{\mathcal{B}_r(0)}$, i.e. when $\mathbf{\Lambda}(\omega)$ is approximated by (77), and the case $\omega \in \mathbb{C}^+_{a,r}$, when (78) is used. We will not present the proof of this result, because it is quite lengthy and technical. It can be found in the report [30].

Theorem 4.1 *Let ρ be like in (80). Then there exists $r_0 > 0$, which depends on ρ, $\boldsymbol{\mu}$, $\boldsymbol{\alpha}$, and the problem in question (Dirichlet or Neumann), s.t. for all $r < r_0$, $N_* \geq N_0$, with N_0 defined in (81), it holds:*

– *for all $\omega \in \mathbb{C}^+ \cap \overline{\mathcal{B}_r(0)}$,*

$$E_{r,N_*}(\omega) < C\left(\frac{r}{\rho}\right)^{2N_*+2}.$$

– *for all $\omega \in \mathbb{C}^+_{a,r}$ (see (82) for notation), with $W = \max(\log|\omega|, 1)$,*

$$E_{r,N_*}(\omega) < C\left(\frac{r}{\rho}\right)^{2N_*+2-n} \gamma^{W^2 + W\log a^{-1}}.$$

The constants $C > 0$, $n \geq 0$, $\gamma > 1$ depend only on ρ, $\boldsymbol{\alpha}$, $\boldsymbol{\mu}$ and the problem (Dirichlet or Neumann) in question.

Proof See [30]. □

Theorem 4.1 shows that in order to ensure that $E_{r,N_*}(\omega) < \varepsilon$, we may fix $r > 0$ sufficiently small, and choose $N_* \geq N_0$, so that, for some $C_* > 0$,

$$N_* \geq C_*\left(\log\varepsilon^{-1} + W\log a^{-1} + W^2\right), \quad W = \max(\log|\omega|, 1). \tag{83}$$

4.2.3 Asymptotic computational complexity of the method of Sect. 4.2.1

In this section we estimate the computational complexity of the procedure **Eval-Lambda**, in terms of ω and the desired accuracy ε. We fix $r > 0$ sufficiently small (cf.

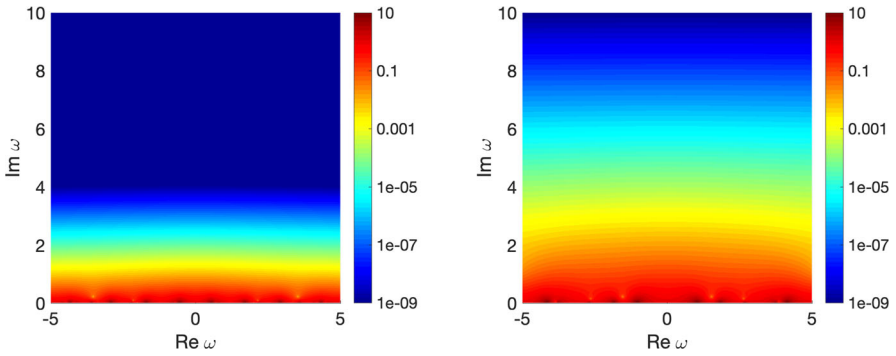

Fig. 3 Left: $|\mathbf{\Lambda}(\omega)\omega^{-1}+i|$ for the Neumann problem, $\boldsymbol{\alpha} = (0.6, 0.8)$, $\boldsymbol{\mu} = (0.8, 0.2)$. Right: $|\mathbf{\Lambda}(\omega)\omega^{-1}+i|$ for the Neumann problem, $\boldsymbol{\alpha} = (0.2, 0.7)$, $\boldsymbol{\mu} = (0.3, 0.3)$. Remark that the color scale is logarithmic

Theorem 4.1), and consider the case when $\omega \in \mathbb{C}^+_{a,r}$, cf. (82), with $0 < a \leq 1$ fixed. First of all, the evaluation of each value in $\mathcal{L}_n$, $n \leq L-1$, requires $O(p) = O(1)$ operations, while to compute each of the values in $\mathcal{L}_L$ we need $O(N_*)$ operations. Thus the total computational cost scales as

$$O\left(\#\bigcup_{n=0}^{L-1}\mathcal{L}_n\right) + O(N_*\#\mathcal{L}_L).$$

With the property (c) from Sect. 4.2.1,

$$\#\bigcup_{n=0}^{L-1}\mathcal{L}_n = \sum_{n=0}^{L-1} C^{p-1}_{n+p-1} = O(L^{p+1}), \quad \#\mathcal{L}_L = O(L^p).$$

When $|\omega| \to +\infty$, L defined in (79) satisfies $L = O(\log|\omega|)$, and the cost $c_{\mathbf{\Lambda}}$ of evaluating $\mathbf{\Lambda}(\omega)$ scales as

$$\begin{aligned} c_{\mathbf{\Lambda}} &= O\left(\log^{p+1}|\omega| + N_*\log^p|\omega|\right) \\ &\overset{(83)}{=} O\left(\log^{p+2}|\omega| + \log^{p+1}|\omega|\log a^{-1}\right) + O\left(\log^p|\omega|\log\varepsilon^{-1}\right). \end{aligned} \tag{84}$$

4.2.4 Approximating $\mathbf{\Lambda}(\boldsymbol{\omega})$ for $\boldsymbol{\omega}$ with large imaginary parts

It appears that when $\operatorname{Im}\omega$ is sufficiently large, $\mathbf{\Lambda}(\omega)$ can be approximated with high accuracy by $-i\omega$ (see Fig. 3 for the numerical illustration).

Theorem 4.2 *There exists $C > 0$, s.t for all $\omega \in \mathbb{C}^+$,*

$$|\mathbf{\Lambda}(\omega) + i\omega| \leq C|\omega|\, \mathrm{e}^{-2\operatorname{Im}\omega}\ \max(1, (\operatorname{Im}\omega)^{-3}). \tag{85}$$

Remark 4.4 When $\omega \in \mathbb{C}^- = \{z \in \mathbb{C} : \operatorname{Im} z < 0\}$, it is possible to show that

$$|\mathbf{\Lambda}(\omega) - i\omega| \le C|\omega| \mathrm{e}^{-2|\operatorname{Im}\omega|} \max(1, |\operatorname{Im}\omega|^{-3}).$$

The proof of the above theorem relies on the following auxiliary result.

Lemma 4.1 *There exist $c, C > 0$, s.t. all $\omega \in \mathbb{C}^+$,*

$$-\operatorname{Im}(\tan\omega)^{-1} \ge c \min(1, \operatorname{Im}\omega), \tag{86}$$

$$\left|1 - i\,(\tan\omega)^{-1}\right| \le C \max(1,\ (\operatorname{Im}\omega)^{-1})\ \mathrm{e}^{-2\operatorname{Im}\omega}. \tag{87}$$

Proof See "Appendix B". □

Proof of Theorem 4.2 Expressing $\mathbf{\Lambda}(\omega)$ via (78), one computes that

$$\mathbf{\Lambda}(\omega) + i\omega = -\omega\left(\mathcal{N}(\omega)/\mathcal{D}(\omega)\right), \tag{88}$$

where, with $\mathbf{F}_{\alpha,\mu}(\omega)$ defined in (78),

$$\begin{cases} \mathcal{N}(\omega) = \left(1 - i(\tan\omega)^{-1}\right)(1 - i\omega^{-1}\mathbf{F}_{\alpha,\mu}(\omega)), \\ \mathcal{D}(\omega) = (\tan\omega)^{-1} + \omega^{-1}\mathbf{F}_{\alpha,\mu}(\omega). \end{cases} \tag{89}$$

Let us first bound the numerator:

$$|\mathcal{N}(\omega)| = \left|1 - i(\tan\omega)^{-1}\right| \left(1 + \sum_{i=0}^{p-1} \mu_i \left|\frac{\mathbf{\Lambda}(\alpha_i\omega)}{\alpha_i\omega}\right|\right).$$

To bound the first term in the product in the right-hand side of the above we use (87), and to bound the second one, we make use of Theorem 2.4(b). Thus,

$$|\mathcal{N}(\omega)| \le C_{\mathcal{N}} \max(1, (\operatorname{Im}\omega)^{-2}) \mathrm{e}^{-2\operatorname{Im}\omega}, \tag{90}$$

where the constant $C_{\mathcal{N}} > 0$ depends on $\boldsymbol{\mu}$ and $\boldsymbol{\alpha}$.

It remains to deal with the denominator. For this we use the bound:

$$|\mathcal{D}(\omega)| \ge |\operatorname{Im}\mathcal{D}(\omega)| \ge \left|\operatorname{Im}(\tan\omega)^{-1} + \sum_{i=0}^{p-1} \mu_i \operatorname{Im}\left((\alpha_i\omega)^{-1}\mathbf{\Lambda}(\alpha_i\omega)\right)\right|.$$

It remains to notice that $\operatorname{Im}(\tan\omega)^{-1}$ and $\operatorname{Im}\left((\alpha_i\omega)^{-1}\mathbf{\Lambda}(\alpha_i\omega)\right)$ are negative for $\operatorname{Im}\omega > 0$, cf. (86) and Theorem 2.4(a). Therefore,

$$|\mathcal{D}(\omega)| \ge \left|\operatorname{Im}(\tan\omega)^{-1}\right| \overset{(86)}{\ge} c \min(1, \operatorname{Im}\omega). \tag{91}$$

Combining the bounds (90) and (91) in (88) yields the desired statement. □

4.3 Computing convolution weights: error, algorithm, complexity

Evaluation of convolution weights based on (74) requires computing $\mathbf{\Lambda}(\omega)$ for a range of complex frequencies ω. We comment on the choice of the parameters ρ and N in (74), see Sect. 4.3.1, discuss how $\mathbf{\Lambda}(\omega)$ is computed within (74) in Sect. 4.3.2 and present some complexity studies in Sect. 4.3.3.

4.3.1 Accuracy of evaluation of convolution weights and choice of ρ, N

Let us relate the accuracy ε of evaluation of $\mathbf{\Lambda}$ as well as the parameters ρ and N in (74) to the numerical error of evaluation of N_t values of $\lambda_n^{\Delta t}$. Because we compute convolution weights for the scaled value of $\mathbf{\Lambda}(\omega)$, namely $\mathbf{\Lambda}^s(\omega) = (-i\omega)^{-1}\mathbf{\Lambda}(\omega)$, see Remark 4.1, we will perform the error analysis for these re-scaled quantities $\lambda_{s,n}^{\Delta t}$, defined as, cf. (27),

$$\mathbf{\Lambda}^s_{\Delta t}(z) = \sum_{n=0}^{\infty} \lambda_{s,n}^{\Delta t} z^n, \quad \mathbf{\Lambda}^s_{\Delta t}(z) = \left(\frac{\delta(z)}{\Delta t}\right)^{-1} \mathbf{\Lambda}\left(i\frac{\delta(z)}{\Delta t}\right). \tag{92}$$

Let us denote by $\mathbf{\Lambda}^{s,\varepsilon}(\omega_k)$ an approximation with an error ε to $\mathbf{\Lambda}^s(\omega_k)$. The convolution weights $\lambda_{s,n}^{\Delta t}$ are computed the help of (74):

$$\begin{aligned} \lambda_{s,n}^{\Delta t} \approx \lambda_{s,n}^{\Delta t,\varepsilon} &:= \frac{\rho^{-n}}{N} \sum_{k=0}^{N-1} \mathrm{e}^{-i\frac{2\pi kn}{N}} \mathbf{\Lambda}^{s,\varepsilon}(\omega_k), \\ \omega_k &= i\frac{\delta\left(\rho \mathrm{e}^{i\frac{2\pi k}{N}}\right)}{\Delta t}, \quad k = 0, \ldots, N_t. \end{aligned} \tag{93}$$

Before analyzing the error induced by the approximation (93), let us show that the exact $\lambda_{s,n}^{\Delta t}$ are bounded. To prove the result that follows, we will use the following observation (see (115) in "Appendix D"):

$$\mathrm{Im}\left(i\frac{\delta(\rho \mathrm{e}^{i\varphi})}{\Delta t}\right) > \frac{1-\rho}{\Delta t}, \quad \varphi \in [0, 2\pi). \tag{94}$$

Proposition 4.2 *The convolution weights satisfy, with some $C > 0$,*

$$\left|\lambda_{s,n}^{\Delta t}\right| \le C \max(1, n\Delta t), \quad n \ge 0. \tag{95}$$

Proof The idea of the proof is from Lemma 5.3, Section 5.1 in [7]. Application of the Cauchy estimate to (28), evaluated for $\ell = n$, with γ being a circle of radius $r_n > 0$ centered in the origin, and $\mathbf{\Lambda}$ replaced by $\mathbf{\Lambda}^s$, yields

$$\left|\lambda_{s,n}^{\Delta t}\right| \le r_n^{-n} \sup_{z \in \partial B_{r_n}(0)} \left| \left(\frac{\delta(z)}{\Delta t}\right)^{-1} \mathbf{\Lambda}\left(i\frac{\delta(z)}{\Delta t}\right) \right|$$

$$\leq r_n^{-n} \sup_{z\in\partial B_{r_n}(0)} \max\left(1, \left(\mathrm{Im}\left(i\frac{\delta(z)}{\Delta t}\right)\right)^{-1}\right),$$

where the last bound follows from Theorem 2.4(b). With (94),

$$\left|\lambda_{s,n}^{\Delta t}\right| \leq r_n^{-n} \max\left(1, \left(\frac{1-r_n}{\Delta t}\right)^{-1}\right).$$

For $n = 0$ the desired result is obtained by choosing $r_0 = 1 - (\Delta t)$. For $n \geq 1$, the choice $r_n = \frac{n}{n+1}$ yields, with $C > 0$,

$$\left|\lambda_{s,n}^{\Delta t}\right| \leq \left(\frac{n+1}{n}\right)^n \max\left(1, (n+1)\Delta t\right) \leq C \max\left(1, n\Delta t\right).$$

□

The error of the approximation (93) is given below.

Proposition 4.3 *Let $0 < \varepsilon < \frac{1}{2}$, $N_t \geq 1$, $N \geq N_t + 1$ be fixed. Assume that $\lambda_{s,n}^{\Delta t,\varepsilon}$, $n = 0, \ldots, N_t$ are given by (93), with $\rho = \varepsilon^{\frac{1}{N+N_t-1}}$. Moreover, assume that*

$$\max_{k=0,\ldots,N-1} \left|\mathbf{\Lambda}^{s,\varepsilon}(\omega_k) - \mathbf{\Lambda}^{s}(\omega_k)\right| < \varepsilon. \tag{96}$$

Then the following error bound holds true, with some $C > 0$:

$$\max_{n=0,\ldots,N_t} \left|\lambda_{s,n}^{\Delta t,\varepsilon} - \lambda_{s,n}^{\Delta t}\right| < C\,(1 + N\Delta t + T)\,\varepsilon^{\frac{N-1}{N+N_t-1}}, \quad T = N_t\Delta t.$$

Proof As the proof is rather classical in CQ theory, and some of its elements appear in various works (cf. e.g. [3,7,38]), we postpone it to "Appendix C". □

It is then obvious that for a given $\varepsilon > 0$, the choice of the parameters

$$N = N_t + 1, \quad \rho = \varepsilon^{\frac{1}{2N_t}}, \tag{97}$$

and ensuring that the inequality (96) holds allows to compute the convolution weights with $O(\sqrt{\varepsilon})$ error:

$$\max_{n=0,\ldots,N_t} \left|\lambda_{s,n}^{\Delta t,\varepsilon} - \lambda_{s,n}^{\Delta t}\right| < C \max(1, T)\sqrt{\varepsilon}.$$

4.3.2 Evaluating convolution weights: algorithmic details

To compute $\mathbf{\Lambda}^{s,\varepsilon}(\omega)$ in (93) that approximate $\mathbf{\Lambda}^{s}(\omega) = (-i\omega)\mathbf{\Lambda}^{s}(\omega)$ with a given precision $\varepsilon > 0$ we use the following strategy, based on the results of Sects. 4.2 and 4.3.1 (here $\gamma_\varepsilon > 0$ is to be fixed later):

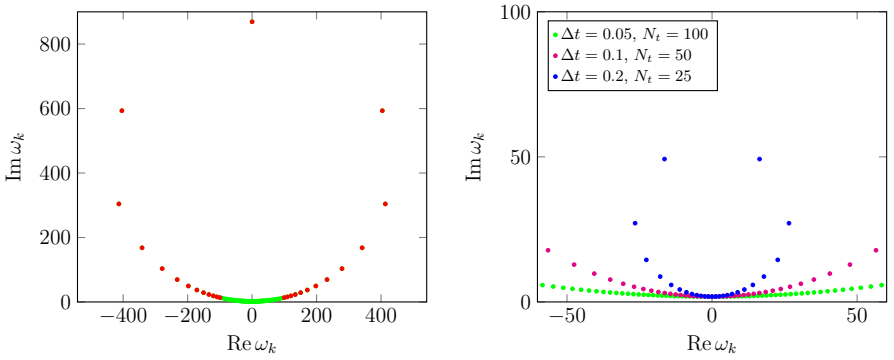

Fig. 4 Left (illustration to Sect. 4.3.2): $N_t = 100$ frequencies ω_k defined in (74), with $\Delta t = 0.05$ and $\rho = \varepsilon^{\frac{1}{2N_t}}$, $\varepsilon = 10^{-8}$. In red we mark ω_k s.t. $\operatorname{Im}\omega_k > \gamma$ (we choose $\gamma = 12$), s.t. $\mathbf{\Lambda}^s(\omega_k)$ is approximated by 1. Right (illustration to Sect. 4.3.3): N_t frequencies ω_k defined in (74) with given Δt, chosen so that $N_t \Delta t = 5$. Remark that in all cases $\operatorname{Im}\omega_k > \text{const}$ (color figure online)

– if $\operatorname{Im}\omega_k < \gamma_\varepsilon$, compute $\mathbf{\Lambda}^{s,\varepsilon}(\omega_k)$ as $(-i\omega_k)^{-1}\mathbf{\Lambda}(\omega_k)$, using the procedure **EvalLambda** for computing $\mathbf{\Lambda}(\omega_k)$. For all ω_k we use the same value of $r > 0$ (sufficiently small) and N_*; the latter is chosen like in (83) with $|\omega| = \max_k\{|\omega_k| : \operatorname{Im}\omega_k < \gamma_\varepsilon\}$ and $a = \min(\min_k \operatorname{Im}\omega_k, 1)$.
– if $\operatorname{Im}\omega_k \geq \gamma_\varepsilon$, take $\mathbf{\Lambda}^{s,\varepsilon}(\omega_k) := 1$, by Theorem 4.2.

Choosing $\gamma_\varepsilon = \frac{1}{2}\log\varepsilon^{-1} + C$, with some $C > 0$, ensures that $\mathbf{\Lambda}^s(\omega) = (-i\omega)^{-1}\mathbf{\Lambda}(\omega)$ is approximated with an accuracy ε, cf. Theorem 4.2. The above strategy is illustrated in Fig. 4 (left).

4.3.3 Complexity estimates

Let us estimate the complexity of the evaluation of (93) in terms of N_t, $\Delta t, \varepsilon$, provided that ρ, N are given by (97). Let us assume that $T = N_t\Delta t$ fixed, and consider the regime $N_t \to \infty$; we also assume that ε is sufficiently small. As discussed in Sect. 4.1, this necessitates a bound on the cost of computing $\mathbf{\Lambda}(\omega_k)$ in (93). This bound, cf. (84), depends on ω_k; thus, we must study how ω_k behaves with N_t, Δt, ε. The following proposition is a minor refinement of some of the results from [3].

Lemma 4.2 *Let ω_k, $k = 0, \ldots, N_t$, $N_t \geq 1$, be given by (93), with N, ρ defined in (97), $\Delta t < 1$ and $0 < \varepsilon < \frac{1}{2}$. Then, with some c, $C > 0$*

$$\text{(a) } \operatorname{Im}\omega_k > c\,\min\left(1, T^{-1}\right),$$
$$\text{(b) } |\omega_k| < CT^{-1}N_t^2.$$

Proof See "Appendix D". □

An illustration to the statement (a) is provided in Fig. 4 (right).

By Lemma 4.2, $\omega_k \in C_{a,a}$, with $a = \min\left(1, c, c/T\right)$. Thus the results of Sect. 4.2.3 about the evaluation of $\mathbf{\Lambda}(\omega)$ apply. The complexity of computation of each of $\mathbf{\Lambda}(\omega_k)$

is $O(1)$ when $\operatorname{Im}\omega_k \geq \gamma_\varepsilon$, and scales as (84) when $\operatorname{Im}\omega_k < \gamma$. Replacing $|\omega_k|$ by $O(N_t^2)$, according to Lemma 4.2, the worst case complexity is given by

$$c_{\mathbf{\Lambda}} = O\left(\log^{p+2} N_t + \log^p N_t \log \varepsilon^{-1}\right).$$

Because (93) requires computing at most $O(N_t)$ values of $\mathbf{\Lambda}(\omega_k)$, and then performing the FFT, see the discussion in Sect. 4.1, the total complexity of computing N convolution weights with an accuracy $O\left(\sqrt{\varepsilon}\right)$ scales as

$$O\left(N_t \log^{p+2} N_t + N_t \log^p N_t \log \varepsilon^{-1}\right).$$

Remark that this complexity scales, in general, better, than $O(N_t^2)$ complexity of the solution of the full problem, cf. Sect. 3.4.

5 Numerical results

In all the numerical results of this section we use the mass-lumped finite element for the space discretization, and a regular spatial grid. This, in particular, implies that the CFL number is $C_{cfl} = \frac{\Delta t}{h}$, cf. (51) and Remark 3.4. In the experiments we fixed r, N_* in the procedure of Sect. 4.2.1 for computation of $\mathbf{\Lambda}(\omega)$ to a (numerically determined) fixed value that allows to approximate $\mathbf{\Lambda}(\omega)$ in the convolution weight computation with a high accuracy. As for the evaluation of the convolution weights, we choose $\varepsilon = 10^{-12}$ in (97).

5.1 Validity of the method

In this section we would like to verify the validity of the transparent boundary conditions constructed in the present article, by comparing a solution computed on the truncated tree to a solution computed on the tree $\mathcal{T}$. However, because the tree $\mathcal{T}$ has infinitely many branches, it is in general impossible to compute such a reference solution. Thus, one of the options would be to truncate the tree up to $\mathcal{N}$ generations, where $\mathcal{N} \gg 1$, and perform the computation on this truncated tree, as it was done e.g. in [33]. Because this is costly, we adapt an alternative approach: given $\mathcal{N}$ generations, we compute the solution to the problem (17) on $\mathcal{T}^m$ with $m = \mathcal{N} - 1$, where we use the transparent boundary conditions approximated with the help of the convolution quadrature. This is the reference solution. We compare this solution with the CQ approximation to (17), where m is fixed, $m < \mathcal{N} - 1$.

Let us remark that no analysis had been made in this article about the convergence of the method with respect to the number of the truncated generations $m + 1$ (a related issue was addressed in [32]).

We solve the Neumann problem on the binary tree $\mathcal{T}$, s.t. the length of the root edge equals to $\ell_{0,0} = 2$, with $\boldsymbol{\alpha} = (0.3, 0.5)$ and $\boldsymbol{\mu} = (1, 0.25)$. The source term is

supported on the root branch of the tree and defined as

$$f(s,t) = 10^6(s-1.5)\mathrm{e}^{-\sigma(s-1.5)^2-\sigma(t-0.1)^2}, \quad \sigma = 5\times 10^3. \tag{98}$$

The reference solution $u_{\mathcal{N}-1}$ is computed on the truncated tree $\mathcal{T}^{\mathcal{N}-1}$ with $\mathcal{N}=5$ generations; $\Delta t = 9.9\times 10^{-5}$, $h = 10^{-4}$. We use the same discretization parameters in all the experiments.

The dependence of the solutions $u_m(s_0,t)$ on t is depicted in Fig. 5; here $s_0 = 1$ is the middle of the root branch. The complex behaviour of the solution is attributed to the multiple reflection phenomena on the tree $\mathcal{T}$: in general, waves are reflected from each of the vertices of the tree. In particular, the second peak of the solution $u_m(s_0,t)$ is due to the wave reflected from the vertex $M_{0,0}$. The first reflections from the infinite boundary of the tree reach $s_0 = 1$ at $t \approx 3.3$. In order to compare quantitatively the approximated solutions u_m computed on the truncated tree with $(m+1)$ generations, where $m = 1, 2, 3$, with the reference solution $u_{\mathcal{N}-1}$, we compute the relative errors by evaluating norms on the first two generations (since 2 is the minimal value for the number of the truncated generations in our experiments):

$$e_m^n = \frac{\left\| u^n_{\mathcal{N}-1} - u^n_m \right\|_{\mathrm{L}^2_\mu(\mathcal{T}^{k-1})}}{\max\limits_{n=0,\dots,N_t} \left\| u^n_{\mathcal{N}-1} \right\|_{\mathrm{L}^2_\mu(\mathcal{T}^{k-1})}}, \quad k=2, \quad e_m := \max\nolimits_{n=0,\dots,N_t} e_m^n. \tag{99}$$

The values e_m are as follows:

$$e_1 \approx 7.1\times 10^{-4}, \quad e_2 \approx 3.7\times 10^{-4} \quad e_3 \approx 1.6\times 10^{-4}.$$

The errors e_m^n as functions of $t^n = n\Delta t$ are shown in Fig. 5, bottom. Numerical experiments indicate that they grow linearly in time; this is not surprising, in view of the results of Theorem 3.6. Figure 5 shows that the errors almost vanish for smaller times (even where the solution is non-zero). This can be explained by the fact that the wave reaches the outer boundary of $\mathcal{T}^m$ (where we use the approximated transparent boundary conditions) and reflects into the tree $\mathcal{T}^1$ (where we measured errors) at $t \approx 1.2$ for $m = 1$, $t \approx 1.6$ for $m = 2$ and $t \approx 1.7$ for $m = 3$.

5.2 Convergence rates and stability

5.2.1 Convergence

We perform the convergence experiments on the tree with $\boldsymbol{\alpha} = (0.2, 0.4)$ and $\boldsymbol{\mu} = (1, 0.25)$, and the length of the root edge $\ell_{0,0} = 2$. Because no closed form solution is, in general, available, we compare the numerical solution computed on a coarse grid $(h,\ \Delta t)$ to the numerical ('reference') solution computed on the finest grid $(h_f,\ \Delta t_f) = (10^{-4}, 0.99\times 10^{-4})$. The solutions are computed on the tree $\mathcal{T}^2$ (i.e. on 3 generations, cf. (2)), on the time interval $(0, T)$, $T = 10$, and with the right hand

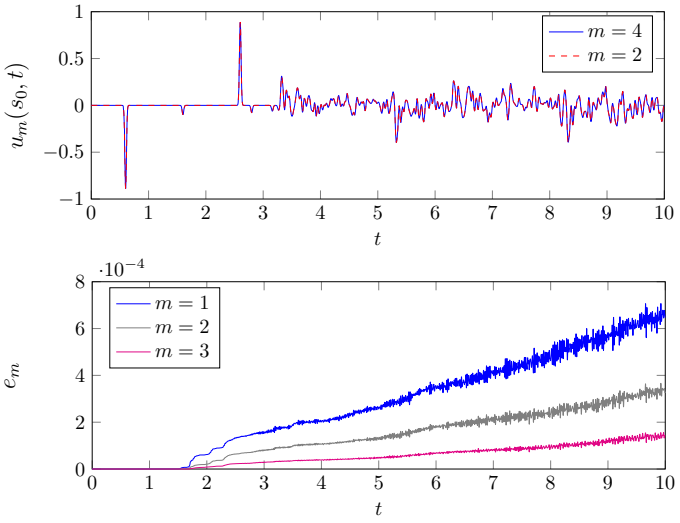

Fig. 5 Top: dependence on t of the numerically approximated solution to the problem (17) $u_m(s_0, t)$ in the point s_0 (which is the middle of the root branch). We study the Neumann problem on the tree with $\ell_{0,0} = 2.0$, $\boldsymbol{\alpha} = (0.3, 0.5)$ and $\boldsymbol{\mu} = (1, 0.25)$, the right hand side (98). Bottom: relative errors e_m^n (cf. (99)) as functions of $t^n = n\Delta t$ (computed for the same experiment)

side supported on the root edge $\Sigma_{0,0}$ and defined by

$$f(s,t) = 10^4 \mathrm{e}^{-100(t-0.75)^2-100(s-1)^2}(s-1).$$

We again consider the Neumann problem. We fix the CFL (51), i.e. the ratio $\frac{\Delta t}{h} = \frac{\Delta t_f}{h_f}$, and perform the experiments on the sequence of grids $(h_k,\ \Delta t_k)$, $1 \le k \le 9$, with $\min_k h_k = 2 \times 10^{-4}$. The reference solution computed at the time t^k is denoted by u_{ref}^k, and the solution on the grid $(h,\ \Delta t)$ by u_h^k. The evolution of the relative error $e_{h,\Delta t}$, defined below, is shown in Fig. 6, left.

$$e_{h,\Delta t} = \max_n e_{h,\Delta t}^n, \quad \text{where } e_{h,\Delta t}^n = \frac{\left\| u_h^n - u_{ref}^n \right\|_{\mathrm{L}^2_\mu(\mathcal{T}^m)}}{\|u_{ref}\|_{\ell^\infty(L^2_\mu(\mathcal{T}^m))}}, \tag{100}$$
$$\|u_{ref}\|_{\ell^\infty(L^2_\mu(\mathcal{T}^m))} := \max_{k=0,\dots,N_t} \left\| u_{ref}^k \right\|_{\mathrm{L}^2_\mu(\mathcal{T}^m)}, \quad N_t = \left\lceil \frac{T}{\Delta t_f} \right\rceil.$$

5.2.2 Long-time stability

To study the stability of the numerical method, we compute the solution to the problem described in Sect. 5.2.1 on the time interval $(0,\ T)$ with $T = 500$, with the discretization $(h,\ \Delta t) = (5 \times 10^{-4}, 4.99 \times 10^{-4})$ (i.e. on around 10^6 time steps). Figure 6, right depicts $\mathrm{L}^2_\mu(\mathcal{T}^2)$-norm of the solution, which clearly stays bounded on the whole time interval.

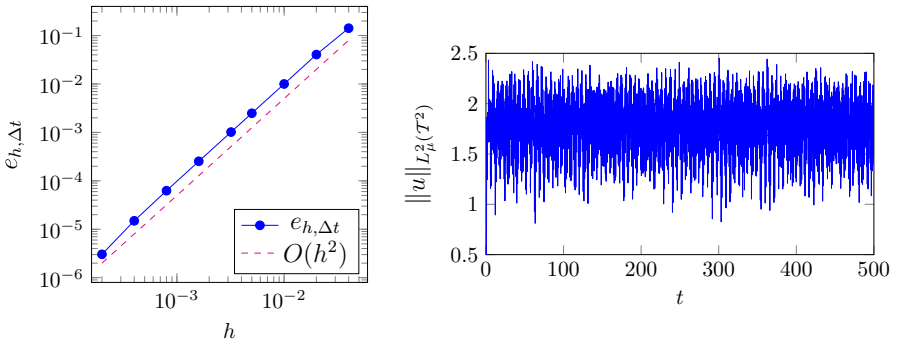

Fig. 6 Left: convergence rates for the experiment of Sect. 5.2.1. Right: dependence on time of the L^2_μ-norm of the solution computed on $\mathcal{T}^2$ in the experiment of Sect. 5.2.2

5.3 Performance of the method on different trees

To explain the experiments that follow, let us provide more information about $\mathbf{\Lambda}(\omega)$. Recall that $\mathbf{\Lambda}(\omega)$ is an even meromorphic in $\mathbb{C}$ function (cf. Theorem 2.4) with real poles. The number of poles of $\mathbf{\Lambda}$ on an interval $(0, \lambda)$ is asymptotically bounded from above by $C\lambda^d$, where $d \geq 1$ and depends on $\boldsymbol{\alpha}$ (see [31]). In particular, when $\sum_i \alpha_i < 1$, one has $d = 1$; while when $\sum_i \alpha_i > 1$, it holds that $d = d_s$, where $d_s > 1$ is a unique number s.t.

$$\sum_{i=0}^{p-1} \alpha_i^{d_s} = 1.$$

Let us remark that in practice these bounds often appear to be optimal. Although the estimates are asymptotic, the difference between these cases is observed already for small λ. In particular, in Fig. 7 we depict numerically computed poles of $\mathbf{\Lambda}(\omega)$ for two sets of parameters: $\boldsymbol{\alpha} = (0.4, 0.4)$, $\boldsymbol{\mu} = (0.5, 1)$ (case $d = 1$) and $\boldsymbol{\alpha} = (0.8, 0.4)$, $\boldsymbol{\mu} = (0.5, 1)$ (case $d = d_s \approx 1.4$).

Our goal is to find out whether the density of poles influences the behaviour of the convolution quadrature. For this we compute the solutions to the Dirichlet and Neumann problems on the reference tree $\mathcal{T}$ (length of its root edge equals $\ell_{0,0} = 1$), constructed with different sets of the parameters, on the time interval $(0, 20)$. As a source we take

$$f(s,t) = 10^6 \mathrm{e}^{-\sigma(s-0.5)^2 - \sigma(t-0.25)^2}(s - 0.5), \quad \sigma = 10^3,$$

supported on the root edge. We repeat the experiment of Sect. 5.2.1, by computing the solutions for different discretizations, the only difference being that we compare the solutions computed on the truncated tree $\mathcal{T}^1$ to the reference solution computed on a fine discretization on the tree $\mathcal{T}^2$. The time interval is chosen so that the reflections from the 'infinite' boundary of the tree are able to reach the computational domain.

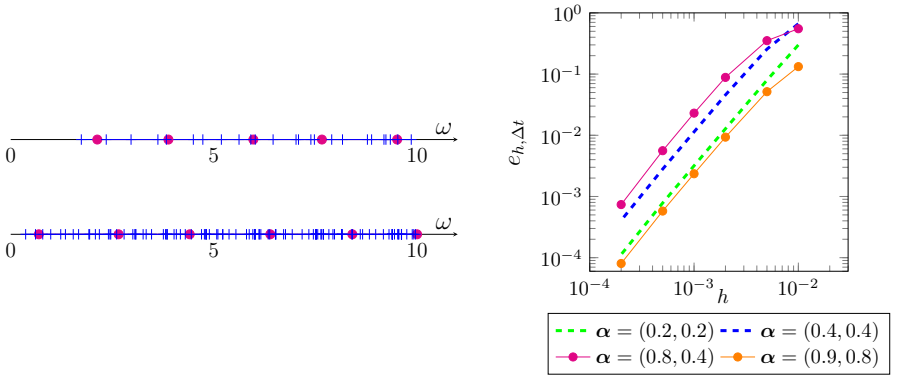

Fig. 7 Left: On top we show the poles of $\mathbf{\Lambda}(\omega)$ on the interval $(0, 10)$ for the Dirichlet problem. Bottom: poles of $\mathbf{\Lambda}(\omega)$ on the interval $(0, 10)$ for the Neumann problem. On both plots with blue vertical dashes we mark the poles corresponding to $\boldsymbol{\alpha} = (0.8, 0.4)$, $\boldsymbol{\mu} = (0.5, 1)$, while with magenta circles the poles corresponding to $\boldsymbol{\alpha} = (0.4, 0.4)$, $\boldsymbol{\mu} = (0.5, 1)$. Right: errors $e_{h,\Delta t}$, cf. (100), for different discretizations for the experiments of Sect. 5.3. In all the experiments $\boldsymbol{\mu} = (0.5, 1.0)$ (color figure online)

The convergence plots for different parameters are shown in Fig. 7, right. In this figure we present the results for the Dirichlet problem only, since in the Neumann case they are very similar. We do not observe any clear correlation between the density of poles of $\mathbf{\Lambda}(\omega)$ and the error behaviour. In particular, the relative errors $e_{h,\Delta t}$ for the parameters $\boldsymbol{\alpha} = (0.8, 0.4)$ (where $d = d_s \approx 1.4$) and $\boldsymbol{\alpha} = (0.4, 0.4)$ (where $d = 1$) are quite close. The same holds true for $\boldsymbol{\alpha} = (0.2, 0.2)$ (the case $d = 1$) and $\boldsymbol{\alpha} = (0.9, 0.8)$ (where $d = d_s \approx 4.42$); let us remark that in this latter case, for the Dirichlet problem, when $\boldsymbol{\alpha} = (0.2, 0.2)$, on the interval $(0, 10)$ there are 3 poles, while when $\boldsymbol{\alpha} = (0.9, 0.8)$, on the interval $(0, 5)$ there are more than 3000 poles.

Let us additionally remark that in the experiment $\boldsymbol{\alpha} = (0.9, 0.8)$ the Dirichlet and Neumann problems coincide, see Theorem 2.2.

Nonetheless, as expected, in these experiments we observe a difference in terms of the computational times (in particular, since the complexity of evaluating $\mathbf{\Lambda}(\omega)$, see Sect. 4.2.3, depends on $|\boldsymbol{\alpha}|_\infty$, this is the case for the convolution weights as well). In the largest computation on the tree $\mathcal{T}^2$, discretized with $h = 10^{-4}$, $\Delta t = 0.99 \times 10^{-4}$, we computed about 2×10^5 convolution weights. On a laptop, this requires about 5 s for the problem with $\boldsymbol{\alpha} = (0.2, 0.2)$, 12 s for $\boldsymbol{\alpha} = (0.4, 0.4)$, 167 s for $\boldsymbol{\alpha} = (0.8, 0.4)$ and almost 12 min for $\boldsymbol{\alpha} = (0.9, 0.8)$. These numbers can be improved by optimizing the parameters in the computations.

6 Conclusions

In this work we approximated the transparent boundary conditions for wave propagation in fractal trees with the help of the convolution quadrature method. Besides stability and convergence analysis, we have additionally considered practical aspects of the algorithm, in particular, computation of the convolution weights. Obtained results, both theoretical and numerical, indicate stability and efficiency of the method.

Nonetheless, some numerical analysis questions remain open (e.g. stability of the problem under perturbation of convolution weights); such analysis may affect some estimates of Sect. 4.3.3 by imposing constraints on the choice of parameters (in particular, the parameter ρ in (74)), cf. e.g. the respective analysis for time-domain boundary integral equations in [7]. We nonetheless believe that the results obtained in this work provide a technical background for continuing the research in this direction.

One of the drawbacks of the CQ method is its complexity, which scales as $O(N_t^2)$ where N_t is the number ot time steps; this is prohibitive when computations on long times are required. This can be overcome using an algorithm similar to the one proposed in [3], see also [4,23]. Additionally, alternative ideas for approximating the transparent boundary conditions, based on the meromorphic expansion of the DtN symbol, are being investigated.

Acknowledgements We are deeply grateful to Adrien Semin (TU Darmstadt, Germany) for providing his code Netwaves.

A Proof of Theorem 2.4

It remains to prove the upper bound on $\mathbf{\Lambda}_{\mathfrak{a}}(\omega)$. Without loss of generality, we will show it for $\mathbf{\Lambda}_{\mathfrak{n}}(\omega)$. First, $\mathbf{\Lambda}_{\mathfrak{n}}(\omega)$ can be defined via the solution of the frequency-domain problem:

$$\mathbf{\Lambda}_{\mathfrak{n}}(\omega) = -\partial_s \lambda(M^*), \quad \omega \in \mathbb{C}^+, \tag{101}$$

where $\lambda \in \mathrm{H}^1_\mu(\mathcal{T})$ solves the boundary-value problem:

$$\omega^2 \int_{\mathcal{T}} \mu(s)\, \lambda\, \overline{v} - \int_{\mathcal{T}} \mu(s)\, \partial_s \lambda\, \partial_s \overline{v} = 0, \quad \text{for all } v \in V_{\mathfrak{n}}, \quad \lambda(M^*) = 1. \tag{102}$$

Let us define $\|v\|_\omega := \int_{\mathcal{T}} \mu \left(|\partial_s v|^2 + |\omega v|^2 \right)$. We proceed as follows:

– first prove the bound $|\mathbf{\Lambda}_{\mathfrak{n}}(\omega)|^2$ by the energy of the solution (notice that $\lambda(M^*) = 1$):

$$|\mathbf{\Lambda}_{\mathfrak{n}}(\omega)|^2 \le |\omega|^2 + C_0(1 + \operatorname{Im}\omega)\|\lambda\|_\omega^2, \quad C_0 > 0. \tag{103}$$

– next show that the energy of the solution is bounded by $\frac{1}{2}|\mathbf{\Lambda}_{\mathfrak{n}}(\omega)|^2$, with C_0 as above:

$$C_0(1 + \operatorname{Im}\omega)\|\lambda\|_\omega^2 \le \frac{1}{2}|\mathbf{\Lambda}_{\mathfrak{n}}(\omega)|^2 + C_1 \max(1, (\operatorname{Im}\omega)^{-2})|\omega|^2, \quad C_1 > 0. \tag{104}$$

– combine (103) and (104) to obtain the desired bound:

$$|\mathbf{\Lambda}_{\mathrm{n}}(\omega)|^2 \leq C \max(1, (\operatorname{Im}\omega)^{-2})|\omega|^2.$$

Proof of the bound (103) Let $v_0(s) = \chi(s)\partial_s\lambda$, where $\chi \in C^1(\mathcal{T};\mathbb{R})$, $\operatorname{supp}\chi(s) \subseteq \Sigma_{0,0}$, $\chi(M^*) = 1$ and $\chi(M_{0,0}) = 0$. The weak formulation (102) implies that λ satisfies

$$\partial_s^2\lambda + \omega^2\lambda = 0 \text{ on } \Sigma_{0,0}.$$

Testing the above with $v_0(s)$, we obtain the following identity on the edge $\Sigma_{0,0}$, parametrized by $s \in [0,1]$ (recall that we work with the reference tree, and thus the length of $\Sigma_{0,0}$ is 1):

$$I_1 + I_2 = 0, \quad \text{where } I_1 = \int_0^1 \partial_s^2\lambda\,\chi(s)\,\partial_s\overline{\lambda}ds, \quad I_2 = \omega^2\int_0^1 \lambda\,\chi(s)\,\partial_s\overline{\lambda}ds. \tag{105}$$

Let $\omega = \omega_r + i\omega_i$, $\omega_r \in \mathbb{R}$ and $\omega_i > 0$. Let us consider the real part of the above:

$$\operatorname{Re} I_1 = \frac{1}{2}\int_0^1 \frac{d}{ds}|\partial_s\lambda|^2\chi(s)ds = -\frac{1}{2}|\mathbf{\Lambda}_{\mathrm{n}}(\omega)|^2 - \frac{1}{2}\int_0^1 \chi'(s)|\partial_s\lambda|^2ds, \tag{106}$$

where in the last identity we used $\chi(0) = 1$ and $\chi(1) = 0$. Combining (105), (106), we deduce

$$|\mathbf{\Lambda}_{\mathrm{n}}(\omega)|^2 \leq 2|\operatorname{Re} I_2| + c_1\int_0^1 |\partial_s\lambda|^2ds, \quad c_1 > 0. \tag{107}$$

Similarly,

$$\begin{aligned}\operatorname{Re} I_2 &= \frac{1}{2}\operatorname{Re}\omega^2\int_0^1 \chi(s)\frac{d}{ds}|\lambda|^2ds - \operatorname{Im}\omega^2\int_0^1 \chi(s)\operatorname{Im}(\lambda\partial_s\overline{\lambda})ds\\ &= -\frac{1}{2}(\omega_r^2 - \omega_i^2) - \frac{1}{2}(\omega_r^2 - \omega_i^2)\int_0^1 \chi'(s)|\lambda|^2ds - 2\omega_i\omega_r\int_0^1 \chi(s)\operatorname{Im}(\lambda\partial_s\overline{\lambda})ds.\end{aligned}$$

where we used $\chi(0) = 1$, $\chi(1) = 0$ and $\lambda(0) = 1$. Applying to the last integral the Young inequality we obtain the following bound, with $c_2, c_3 > 0$,

$$|\operatorname{Re} I_2| \leq \frac{1}{2}|\omega|^2 + c_2|\omega|^2 \int_0^1 |\lambda|^2 ds + c_3\omega_i \left(|\omega_r|^2 \int_0^1 |\lambda|^2 ds + \int_0^1 |\partial_s \lambda|^2 ds \right). \tag{108}$$

Inserting (108) into (107) we prove (103).

Proof of the bound (104) Testing the Helmholtz equation corresponding to (102) with $\omega\lambda(s)$ and integrating by parts we obtain the following identity (recall that $\lambda(M^*) = 1$):

$$\overline{\omega}\mathbf{\Lambda}_{\mathfrak{n}}(\omega) = \overline{\omega} \int_{\mathcal{T}} \mu|\partial_s\lambda|^2 - |\omega|^2\omega \int_{\mathcal{T}} \mu|\lambda|^2.$$

Taking the imaginary part of the above results in

$$\operatorname{Im}(\overline{\omega}\mathbf{\Lambda}_{\mathfrak{n}}(\omega)) = -\omega_i \left(\int_{\mathcal{T}} \mu|\partial_s\lambda|^2 + |\omega|^2 \int_{\mathcal{T}} \mu|\lambda|^2 \right) = -\omega_i \|\lambda\|_{\omega}^2.$$

Multiplying both sides of the above by $-C_0(1+\omega_i)\omega_i^{-1}$, with C_0 is as in (103), we obtain

$$-C_0\left(\omega_i^{-1} + 1\right) \operatorname{Im}(\overline{\omega}\mathbf{\Lambda}_{\mathfrak{n}}(\omega)) = C_0(1+\omega_i)\|\lambda\|_{\omega}^2. \tag{109}$$

It suffices to notice that the left hand side in the above equality is bounded:

$$\begin{aligned} &\left| -C_0\left(\omega_i^{-1} + 1\right) \operatorname{Im}(\overline{\omega}\mathbf{\Lambda}_{\mathfrak{n}}(\omega)) \right| \\ &\quad \leq C_0\left(\omega_i^{-1} + 1\right)|\omega||\mathbf{\Lambda}_{\mathfrak{n}}(\omega)| \leq \frac{1}{2}|\mathbf{\Lambda}_{\mathfrak{n}}(\omega)|^2 + \frac{C_0^2}{2}\left(\omega_i^{-1} + 1\right)^2 |\omega|^2, \end{aligned}$$

where we used the Young inequality. In the above we bound further $C_0(\omega_i^{-1} + 1) \leq 2\max(1, \omega_i^{-1})$. Inserting the bound into (109) gives

$$C_0(1+\omega_i)\|\lambda\|_{\omega}^2 \leq \frac{1}{2}|\mathbf{\Lambda}_{\mathfrak{n}}(\omega)|^2 + 2C_0^2 \max\left(1, \omega_i^{-2}\right)|\omega|^2,$$

i.e. (104). Combining (103) and (104) proves the statement of the theorem.

B Proof of Lemma 4.1

We first show (86). By definition, $\tan\omega = i\frac{1-z}{1+z}$, with $z = \mathrm{e}^{2i\omega}$, $\omega = \omega_r + i\omega_i$. Then,

$$
\begin{aligned}
-\operatorname{Im}(\tan\omega)^{-1} &= \operatorname{Re}\frac{1+z}{1-z} = \operatorname{Re}\frac{(1+z)(1-\overline{z})}{|1-z|^2} = \frac{1-|z|^2}{1+|z|^2-2\operatorname{Re} z} \geq \frac{1-|z|^2}{(1+|z|)^2} \\
&= \frac{1-|z|}{1+|z|} = \frac{1-\mathrm{e}^{-2\omega_i}}{1+\mathrm{e}^{-2\omega_i}} \geq \begin{cases} \frac{\mathrm{e}^{2\omega_i}-1}{\mathrm{e}^{2\omega_i}+1} \geq \frac{2\omega_i}{\mathrm{e}^2+1}, & \text{if } 0 < \omega_i \leq 1, \\ \frac{1-\mathrm{e}^{-2}}{1+\mathrm{e}^{-2}}, & \text{if } \omega_i > 1, \end{cases}
\end{aligned}
\tag{110}
$$

hence the bound (86). Let us show (87). After straightforward computations,

$$
\left|1 - i\,(\tan\omega)^{-1}\right| = \frac{2|z|}{|1-z|} \leq \frac{2|z|}{|1-|z||} = \frac{2\mathrm{e}^{-2\omega_i}}{1-\mathrm{e}^{-\omega_i}} \leq C\max\left(1, \omega_i^{-1}\right)\mathrm{e}^{-2\omega_i},
$$

where the last bound follows by noticing that, for $\omega_i > 0$,

$$
1 - \mathrm{e}^{-\omega_i} \geq \begin{cases} 1-\mathrm{e}^{-1}, & \text{if } \omega_i \geq 1, \\ \mathrm{e}^{-1}\omega_i, & \text{if } \omega_i < 1 \end{cases} \quad \geq c\min(1, \omega_i), \quad c > 0. \tag{111}
$$

C Proof of Proposition 4.3

To prove Proposition 4.3, we need the following auxiliary result.

Lemma C.1 *Let $0 < \rho < 1$, $\varepsilon > 0$, and $\lambda_{s,n}^{\Delta t,\varepsilon}$, $n = 0, \ldots, N_t$ be given by (93), with $N \geq N_t + 1$, where $\max_k \left|\mathbf{\Lambda}^{s,\varepsilon}(\omega_k) - \mathbf{\Lambda}^{s}(\omega_k)\right| < \varepsilon$. Then*

$$
\begin{aligned}
&\max_{n=0,\ldots,N_t} \left|\lambda_{s,n}^{\Delta t,\varepsilon} - \lambda_{s,n}^{\Delta t}\right| < \rho^{-N_t}\varepsilon + \rho^N C_N(\rho), \\
&C_N(\rho) = (1-\rho^N)^{-1}\left(1 + N_t\Delta t + N\Delta t(1-\rho^N)^{-1}\right).
\end{aligned}
\tag{112}
$$

Proof For all $n = 0, \ldots, N_t$,

$$
\begin{aligned}
\left|\lambda_{s,n}^{\Delta t,\varepsilon} - \lambda_{s,n}^{\Delta t}\right| &\leq S_1 + S_2, \\
S_1 &= \left|\frac{\rho^{-n}}{N}\sum_{k=0}^{N-1} \mathrm{e}^{-i\frac{2\pi kn}{N}}\left(\mathbf{\Lambda}^{s,\varepsilon}(\omega_k) - \mathbf{\Lambda}^{s}(\omega_k)\right)\right|, \\
S_2 &= \left|\frac{\rho^{-n}}{N}\sum_{k=0}^{N-1} \mathrm{e}^{-i\frac{2\pi kn}{N}}\mathbf{\Lambda}^{s}(\omega_k) - \lambda_{s,n}^{\Delta t}\right|.
\end{aligned}
\tag{113}
$$

An upper bound for S_1 follows from the triangle inequality and the assumption of the proposition: $S_1 \leq \rho^{-n}\varepsilon \leq \rho^{-N_t}\varepsilon$ (because $\rho < 1$).

As for S_2, it suffices to replace $\mathbf{\Lambda}^s(\omega_k)$ in the above sum by $\sum_{\ell=0}^{\infty}\lambda_{s,\ell}^{\Delta t}\rho^\ell e^{i\frac{2\pi\ell k}{N}}$, cf. (92), and use the aliasing argument. In particular,

$$\frac{\rho^{-n}}{N}\sum_{k=0}^{N-1} e^{-i\frac{2\pi kn}{N}}\mathbf{\Lambda}^s(\omega_k) = \frac{\rho^{-n}}{N}\sum_{k=0}^{N-1}\sum_{\ell=0}^{\infty}\lambda_{s,\ell}^{\Delta t}\,\rho^\ell\, e^{i\frac{2\pi k(\ell-n)}{N}}.$$

Since $N^{-1}\sum_{k=0}^{N-1} e^{i\frac{2\pi k(\ell-n)}{N}} = 1$ when $\ell-n$ is a multiple of N and vanishes otherwise, and $n \le N_t \le N-1$, the above can be rewritten as follows:

$$\frac{\rho^{-n}}{N}\sum_{k=0}^{N-1} e^{-i\frac{2\pi kn}{N}}\mathbf{\Lambda}^s(\omega_k) = \lambda_{s,n}^{\Delta t} + \rho^{-n}\sum_{k=1}^{\infty}\lambda_{s,kN+n}^{\Delta t}\rho^{kN+n}, \quad \text{and}$$

$$S_2 \le \rho^{-n}\sum_{k=1}^{\infty}\left|\lambda_{s,n+kN}^{\Delta t}\right|\rho^{n+kN} \overset{(95)}{\le} C\sum_{k=1}^{\infty}\max(1,(n+kN)\Delta t)\rho^{kN}.$$

The above sum is then bounded:

$$\begin{aligned} S_2 &\le \sum_{k=1}^{\infty}\rho^{kN} + \sum_{k=1}^{\infty}\rho^{kN}(n+kN)\Delta t \\ &\le \rho^N(1-\rho^N)^{-1}(1+n\Delta t) + N\Delta t\,\rho^N(1-\rho^N)^{-2}. \end{aligned}$$

The result follows by bounding in the above $n\Delta t$ by $N_t\Delta t$ and combining bounds for S_1 and S_2 into (113). □

The bound of Lemma C.1 allows us to quantify the choice of ρ, N in (93).

Proof of Proposition 4.3 The desired bound follows by applying the result of Lemma C.1. In particular, $C_N(\rho)$ can be estimated by providing an adequate estimate on $1-\rho^N = 1-\varepsilon^{\frac{N}{N+N_t-1}}$. Because $N_t \ge 1$, the function $N \mapsto 1-\varepsilon^{\frac{N}{N+N_t-1}} = 1-\varepsilon\varepsilon^{\frac{1-N_t}{N+N_t-1}}$ grows in N. Since, additionally, $N \ge N_t+1$, we have

$$1-\rho^N \ge 1-\varepsilon^{\frac{N_t+1}{2N_t}} > 1-\sqrt{\varepsilon} > 1-\sqrt{\frac{1}{2}}, \text{ for all } 0<\varepsilon<\frac{1}{2}.$$

Plugging in this bound into (112) yields $C_N(\rho) \le C(1+(N+N_t)\Delta t)$ and

$$\max_{n=0,\dots,N_t}|\lambda_{s,n}^{\Delta t,\varepsilon} - \lambda_{s,n}^{\Delta t}| < \varepsilon^{\frac{N-1}{N+N_t-1}} + C\varepsilon^{\frac{N}{N+N_t-1}}(1+(N+N_t)\Delta t),$$

from which the desired bound is obtained immediately. □

D Proof of Lemma 4.2

Let us show (a), which basically follows from Section 5.2.1 in [3]. The frequencies ω_k defined in (74), namely,

$$\omega_k = i\frac{\delta\left(\rho e^{i\frac{2\pi k}{N}}\right)}{\Delta t} = \frac{2i}{\Delta t}\frac{1-\rho e^{i\varphi_k}}{1+\rho e^{i\varphi_k}}, \quad \varphi_k = e^{i\frac{2\pi k}{N}},$$

lie on the circle centered at $c_{\rho,\Delta t}$ of radius $R_{\rho,\Delta t}$ (this follows from the fact that $z \mapsto \frac{1-z}{1+z}$ is a homography), with

$$c_{\rho,\Delta t} = \frac{2i}{\Delta t}\frac{1+\rho^2}{1-\rho^2}, \quad R_{\rho,\Delta t} = \frac{2}{\Delta t}\frac{2\rho}{1-\rho^2}, \tag{114}$$

i.e. $\omega_k = c_{\rho,\Delta t} + R_{\rho,\Delta t}e^{i\psi_k}$, for some $\psi_k \in [0, 2\pi)$. Hence

$$\operatorname{Im}\omega_k \geq \inf_{0\leq\varphi<2\pi} \operatorname{Im}\left(i\frac{\delta(\rho e^{i\varphi})}{\Delta t}\right) = \frac{2}{\Delta t}\frac{1+\rho^2-2\rho}{1-\rho^2} = \frac{2}{\Delta t}\frac{1-\rho}{1+\rho}, \tag{115}$$

and, as $\rho < 1$, $\operatorname{Im}\omega_k > \frac{1-\rho}{\Delta t}$. For ρ defined in (97),

$$1-\rho = 1-\varepsilon^{\frac{1}{2N_t}} = 1-\exp\left(-\frac{\log\varepsilon^{-1}}{2N_t}\right) > c_0\min\left(1, \frac{\log\varepsilon^{-1}}{N_t}\right), \quad c_0 > 0, \tag{116}$$

where the last bound follows from (111). Therefore, as $\Delta t < 1$, and $\varepsilon < \frac{1}{2}$,

$$\operatorname{Im}\omega_k > c\min\left(1, \frac{1}{N_t\Delta t}\right), \quad c > 0.$$

To show (b), we use the same property (114), which results in

$$|\omega_k| \leq \frac{2}{\Delta t}\left(\frac{1+\rho^2}{1-\rho^2} + \frac{2\rho}{1-\rho^2}\right) \leq \frac{2(1+\rho)}{\Delta t(1-\rho)} < \frac{4}{\Delta t(1-\rho)}.$$

Using (116), and then $\varepsilon < \frac{1}{2}$, we deduce the following inequality, for some $C, C' > 0$,

$$|\omega_k| < \frac{C}{\Delta t}\max\left(1, N_t\left(\log\varepsilon^{-1}\right)^{-1}\right) \leq \frac{C'}{\Delta t}\max(1, N_t) \leq \frac{C'}{N_t\Delta t}N_t^2.$$

□

References

1. Arioli, M., Benzi, M.: A finite element method for quantum graphs. IMA J. Numer. Anal. **38**(3), 1119–1163 (2018)
2. Arnold, A., Ehrhardt, M., Sofronov, I.: Discrete transparent boundary conditions for the Schrödinger equation: fast calculation, approximation, and stability. Commun. Math. Sci. **1**(3), 501–556 (2003)
3. Banjai, L.: Multistep and multistage convolution quadrature for the wave equation: algorithms and experiments. SIAM J. Sci. Comput. **32**(5), 2964–2994 (2010)
4. Banjai, L., Kachanovska, M.: Fast convolution quadrature for the wave equation in three dimensions. J. Comput. Phys. **279**, 103–126 (2014)
5. Banjai, L., Lubich, C.: Runge–Kutta convolution coercivity and its use for time-dependent boundary integral equations. IMA J. Numer. Anal. **39**(3), 1134–1157 (2019)
6. Banjai, L., Lubich, C., Sayas, F.J.: Stable numerical coupling of exterior and interior problems for the wave equation. Numer. Math. **129**(4), 611–646 (2015)
7. Banjai, L., Sauter, S.: Rapid solution of the wave equation in unbounded domains. SIAM J. Numer. Anal. **47**(1), 227–249 (2008/09)
8. Berkolaiko, G., Kuchment, P.: Introduction to Quantum Graphs, Mathematical Surveys and Monographs, vol. 186. American Mathematical Society, Providence (2013)
9. Besse, C., Ehrhardt, M., Lacroix-Violet, I.: Discrete artificial boundary conditions for the linearized Korteweg–de Vries equation. Numer. Methods Partial Differ. Equ. **32**(5), 1455–1484 (2016)
10. Besse, C., Mésognon-Gireau, B., Noble, P.: Artificial boundary conditions for the linearized Benjamin–Bona–Mahony equation. Numer. Math. **139**(2), 281–314 (2018)
11. Besse, C., Noble, P., Sanchez, D.: Discrete transparent boundary conditions for the mixed KDV–BBM equation. J. Comput. Phys. **345**, 484–509 (2017)
12. Cazeaux, P., Grandmont, C., Maday, Y.: Homogenization of a model for the propagation of sound in the lungs. Multiscale Model. Simul. **13**(1), 43–71 (2015)
13. Cazeaux, P., Hesthaven, J.S.: Multiscale modelling of sound propagation through the lung parenchyma. ESAIM Math. Model. Numer. Anal. **48**(1), 27–52 (2014)
14. Chabassier, J., Imperiale, S.: Introduction and study of fourth order theta schemes for linear wave equations. J. Comput. Appl. Math. **245**, 194–212 (2013)
15. Cohen, G., Pernet, S.: Finite Element and Discontinuous Galerkin Methods for Transient Wave Equations, Scientific Computation. Springer, Dordrecht (2017). With a foreword by Patrick Joly
16. Dai, Z., Peng, Y., Mansy, H.A., Sandler, R.H., Royston, T.J.: Experimental and computational studies of sound transmission in a branching airway network embedded in a compliant viscoelastic medium. J. Sound Vib. **339**, 215–229 (2015)
17. Domínguez, V., Sayas, F.J.: Some properties of layer potentials and boundary integral operators for the wave equation. J. Integral Equ. Appl. **25**(2), 253–294 (2013)
18. Ern, A., Guermond, J.L.: Theory and Practice of Finite Elements, vol. 159. Springer, Berlin (2013)
19. Eruslu, H., Sayas, F.J.: Brushing up a theorem by Lehel Banjai on the convergence of Trapezoidal Rule Convolution Quadrature. arXiv e-prints arXiv:1903.09031 (2019)
20. Eruslu, H., Sayas, F.J.: Polynomially bounded error estimates for Trapezoidal Rule Convolution Quadrature. Comput. Math. Appl. **79**(6), 1634–1643 (2020)
21. Grandmont, C., Maury, B., Meunier, N.: A viscoelastic model with non-local damping application to the human lungs. M2AN Math. Model. Numer. Anal. **40**(1), 201–224 (2006)
22. Gruhne, V.: Numerische Behandlung zeitabhängiger akustischer Streuung im Außen- und Freiraum. Ph.D. thesis, University of Leipzig (2013)
23. Hairer, E., Lubich, C., Schlichte, M.: Fast numerical solution of nonlinear Volterra convolution equations. SIAM J. Sci. Stat. Comput. **6**(3), 532–541 (1985)
24. Hassell, M.E., Sayas, F.J.: A fully discrete BEM–FEM scheme for transient acoustic waves. Comput. Methods Appl. Mech. Eng. **309**, 106–130 (2016)
25. Henry, B.: The Audible Human Project: geometric and acoustic modeling in the airways, lungs and torso. Ph.D. thesis (2018)
26. Henry, B., Royston, T.J.: A multiscale analytical model of bronchial airway acoustics. J. Acoust. Soc. Am. **4**(142), 1774–1783 (2017)
27. Imperiale, S.: Modélisation mathématique et numérique de capteurs piézoélectriques. Ph.D. thesis, Université Paris Dauphine (2012). http://www.theses.fr/2012PA090003. Accessed 8 Nov 2017

28. Johnson, C., Nédélec, J.C.: On the coupling of boundary integral and finite element methods. Math. Comput. **35**(152), 1063–1079 (1980)
29. Joly, P.: Variational methods for time-dependent wave propagation problems. In: Ainsworth, M., Davies, P., Duncan, D., Martin, P., Rynne, B. (eds.) Topics in Computational Wave Propagation. Direct and Inverse Problems. Lecture Notes in Computational Science and Engineering, vol. 31. Springer-Verlag, Berlin (2003)
30. Joly, P., Kachanovska, M.: Transparent boundary conditions for wave propagation in fractal trees: convolution quadrature approach (extended report) (2019). https://hal.archives-ouvertes.fr/hal-02265345. Accessed 3 Aug 2020
31. Joly, P., Kachanovska, M.: Local transparent boundary conditions for wave propagation in fractal trees (II). Error and complexity analysis (2020). https://hal.archives-ouvertes.fr/hal-02909750. Accessed 3 Aug 2020
32. Joly, P., Kachanovska, M.: Local transparent boundary conditions for wave propagation in fractal trees (I). Method and numerical implementation (2020). https://hal.archives-ouvertes.fr/hal-02462264. Accessed 3 Aug 2020
33. Joly, P., Kachanovska, M., Semin, A.: Wave propagation in fractal trees. Mathematical and numerical issues. Netw. Heterog. Media **14**(2), 205–264 (2019)
34. Joly, P., Semin, A.: Construction and analysis of improved Kirchoff conditions for acoustic wave propagation in a junction of thin slots. In: Paris-Sud Working Group on Modelling and Scientific Computing 2007–2008, ESAIM Proceedings, vol. 25, pp. 44–67. EDP Sciences, Les Ulis (2008)
35. Kazakova, M., Noble, P.: Discrete transparent boundary conditions for the linearized Green–Naghdi system of equations. SIAM J. Numer. Anal. **58**(1), 657–683 (2020)
36. Kovács, B., Lubich, C.: Stable and convergent fully discrete interior–exterior coupling of Maxwell's equations. Numer. Math. **137**(1), 91–117 (2017)
37. Lubich, C.: Convolution quadrature and discretized operational calculus. Numer. Math. I. **52**(2), 129–145 (1988)
38. Lubich, C.: Convolution quadrature and discretized operational calculus. Numer. Math. II **52**(4), 413–425 (1988)
39. Maury, B.: The Respiratory System in Equations. Springer, Berlin (2013)
40. Maury, B., Salort, D., Vannier, C.: Trace theorems for trees, application to the human lungs. Netw. Heterog. Media **4**(3), 469–500 (2009)
41. Melenk, J.M., Rieder, A.: Runge–Kutta convolution quadrature and FEM–BEM coupling for the time-dependent linear Schrödinger equation. J. Integral Equ. Appl. **29**(1), 189–250 (2017)
42. Nelson, T.R., West, B.J., Goldberger, A.L.: The fractal lung: universal and species-related scaling patterns. Experientia **46**(3), 251–254 (1990)
43. Pazy, A.: Semigroups of Linear Operators and Applications to Partial Differential Equations, Applied Mathematical Sciences, vol. 44. Springer, New York (1983)
44. Royston, T.J., Zhang, X., Mansy, H.A., Sandler, R.H.: Modeling sound transmission through the pulmonary system and chest with application to diagnosis of a collapsed lung. J. Acoust. Soc. Am. **111**(4), 1931–1946 (2002)
45. Schädle, A.: Non-reflecting boundary conditions for the two-dimensional Schrödinger equation. Wave Motion **35**(2), 181–188 (2002)
46. Semin, A.: Propagation d'ondes dans des jonctions de fentes minces. Ph.D. thesis, Université Paris-Sud (2010)
47. The Audible Human Project of Acoustics and Vibrations Laboratory of University of Illinois at Chicago (2007–2014). http://acoustics.mie.uic.edu/ahp/htdocs/default.php. Accessed 3 Aug 2020
48. Weibel, E.R.: Morphometry of the Human Lung. Springer, Berlin (1963)